tion, and differentiation of cells from mononuclear phagocyte lineage.[11]

Expression of VEGF in the heart has been documented,[12,13] and cardiomyocytes have been reported as a major source of VEGF in the heart.[12] Skeletal muscles expressed VEGF,[13,14] and M-CSF increased VEGF production from skeletal muscles *in vivo* and *in vitro*,[14] but it is unknown whether M-CSF increases VEGF production from cardiomyocytes. M-CSF treatment increased serum VEGF levels in mice,[14] and the level was in the potentially therapeutic range that could treat ischemic diseases in human patients.[15]

Erythropoietin and G-CSF directly protected cardiomyocytes from cell death stimulation.[4,6] M-CSF improves the survival of mononuclear phagocyte lineage cells,[11] but the cell survival effect of M-CSF on cardiomyocytes is unknown. As for their signaling pathways, M-CSF activates Akt, extracellular signal-regulated kinase (ERK), and/or Janus-associated kinase (Jak)-signal transducer and activator of transcription (STAT) cell signaling pathways in bone marrow-derived macrophages and macrophage cell lines.[16–18] M-CSF increased VEGF production in skeletal muscles via Akt activation *in vitro*.[14] However, the cell signaling pathways of M-CSF in cardiomyocytes have not been investigated.

In the present study, we investigated the angiogenic and protective effects of M-CSF on cardiomyocytes *in vitro* and *in vivo*, in mice, rats, and goats. We show that M-CSF increases VEGF production in cardiomyocytes via Akt activation, directly protects cultured cardiomyocytes and myotubes from cell death stimulation by Akt and ERK activation and by up-regulation of downstream anti-apoptotic protein Bcl-xL. Moreover, we show the benefits of M-CSF treatment for ischemic heart diseases *in vivo* using goats as a large animal model.

Materials and Methods

Reagents and Cell Culture

Human M-CSF (Kyowa Hakko Kogyo, Tokyo, Japan) was dissolved in saline for goat experiments described below or in phosphate-buffered saline (PBS) for other experiments. Phycoerythrin-labeled anti-M-CSF receptor (M-CSF-R) monoclonal antibody, control rat IgG2a, and unlabeled anti-CD16/32 monoclonal antibody were purchased from eBioscience (San Diego, CA). H9c2 cells (American Type Culture Collection, Manassas, VA) were cultured in high-glucose Dulbecco's modified Eagle's medium containing 10% fetal calf serum, 100 U/ml penicillin, and 0.1 mg/ml streptomycin (growth medium, GM). To induce cardiac differentiation, H9c2 myoblasts were cultured in differentiation medium (DM) with daily supplementation of 10 nmol/L *all-trans*-retinoic acid (ATRA) (Sigma, St. Louis, MO), with medium changed every 2 days.[19] The difference between GM and DM is 1% fetal calf serum in DM. H9c2 myoblasts were differentiated to myotubes by culturing in the same DM for 11 days.[20] Mouse primary cardiomyocytes were obtained from 1- to 3-day-old neonatal C57BL/6 mice.[21] Heart ventricles were washed in ice-cold Hanks' balanced salt solution without either Ca^{2+} or Mg^{2+} and then minced. The cells were dissociated with 0.25% trypsin in Hanks' balanced salt solution. The supernatants were collected every 15 minutes and centrifuged. To exclude nonmuscle cells, the cells were cultured at 37°C for 2 hours. Then the suspended cells were collected and cultured at 1×10^5 cells/cm^2. After 48 hours, more than 90% of the cells were considered as cardiomyocytes by cross-striation structure staining with Bodipy FL phallacidin (Molecular Probes, Eugene, OR).

Cell Proliferation and Cell Death Assays

H9c2 cells (5×10^3 cells) were plated on 96-well plates and differentiated to cardiomyocytes or myotubes, and the assays were performed as previously shown.[22] For proliferation assays, H9c2 cardiomyocytes or myotubes were treated with M-CSF for indicated time periods, and the cell numbers were counted by a water-soluble tetrazolium (WST) assay using a cell counting kit (Dojindo, Tokyo, Japan). For cell death assays, differentiated H9c2 cells were incubated with M-CSF in the presence or absence of PD98059 (at 30 or 6 μmol/L; Biosource, Camarillo, CA) or LY294002 (at 10 or 2 μmol/L; Biosource) for 24 hours. Then the cells were stimulated with indicated amount of H_2O_2 for 8 hours. The cell viability was determined by the WST assay.

Flow Cytometry

The cells were incubated with unlabeled anti-CD16/32 monoclonal antibody to block nonspecific binding and then with phycoerythrin-labeled antibodies. Flow cytometry was performed with a FACScan (BD Bioscience, San Jose, CA).[14]

Histology

The goat hearts were fixed in 10% formalin, embedded in paraffin, and sectioned. The sections were stained with hematoxylin and eosin (H&E) or Masson's elastic stain. The microvessel density in myocardial infarction lesions was determined as previously shown by immunohistochemical staining of goat hearts with polyclonal rabbit anti-human factor VIII-related antigen antibody (DakoCytomation, Carpinteria, CA) at 1:200 dilution.[14,23] The applicability of this antibody to goats was previously reported.[24] The image with the highest microvessel density was chosen at ×100 magnification, and the vessels were counted at ×200 magnification. Two independent investigators counted at least four fields for each section, and the highest count was taken. To quantify the infarct area, a standard point-counting technique was used as previously described with minor modifications.[25] In brief, the whole heart cross section with highest infarct area was selected, and a 200-point grid was superimposed onto each captured image using Adobe Photoshop (Adobe Systems Inc., San Jose, CA). The area fraction of infarction was

calculated by dividing the number of infarct points by the total number of points falling on the tissue section and was expressed as a percentage.

Western Blot Analysis

Western blot analysis was performed as shown previously.[26] H9c2 myoblasts (5×10^6 cells) were cultured in GM on day 0. From day 1, the cells were differentiated to cardiomyocytes or myotubes. After differentiation, the cells were serum-starved for 6 hours and stimulated with M-CSF. For inhibitor experiments, the cells were cultured with inhibitors for 30 minutes and then stimulated with M-CSF and inhibitors. PD98059 was incubated at a concentration of 30 or 6 μmol/L, and LY294002 was incubated at a concentration of 10 or 2 μmol/L. The cell lysates were subjected to 12% sodium dodecyl sulfate-polyacrylamide gel electrophoresis and transferred onto polyvinylidene difluoride membranes (Millipore, Billerica, MA). The membranes were blotted with antibodies to phospho-ERK, phospho-Akt, phospho-Stat1, phospho-Stat3, phospho-Bad, Bcl-xL (Cell Signaling Technology, Beverly, MA), phospho-Jak1, or M-CSF-R (Santa Cruz Biotechnology, Santa Cruz, CA). The membranes blotted with antibodies to detect phosphorylation were then reblotted with antibodies to total ERK, Akt, Stat1, Stat3, Bad (Cell Signaling Technology), or Jak1 (Santa Cruz Biotechnology).

Mouse and Goat Preparation

The Laboratory Animal Committee at Tohoku University approved all animal experiments. Male C57BL/6 mice, 7 to 9 weeks old, were injected intramuscularly with M-CSF (200 μg/kg body weight) or PBS (control) for 3 consecutive days ($n = 5$ per group). Adult male goats (48 to 53 kg body weight) were intubated and anesthetized with 2% halothane as previously reported ($n = 3$ per group).[27] The goats were incised between the fourth and fifth ribs, and a left lateral thoracotomy was performed. Myocardial infarction was induced by left anterior descending coronary artery ligation with some modifications.[28] For the permanent left anterior descending coronary artery ligation model, left anterior descending coronary artery was ligated at a point ~60% from the beginning of the left coronary artery to the apex. M-CSF (40 μg/kg body weight) intravenous injection began just after the ligation and continued daily for 13 days; on day 14, the goats were anesthetized with 2% halothane and sacrificed. Control goats were injected with saline. For the ischemia-reperfusion model, M-CSF was injected intravenously for 3 consecutive days. Then the left anterior descending coronary artery was ligated at a point ~40% from the beginning of the left coronary artery to the apex for 30 minutes followed by reperfusion.[5] A micromanometer tipped catheter (Millar Instruments Inc., Houston, TX) was positioned in the left ventricle (LV). Hemodynamic parameters were recorded using a data recording unit (TEAC Corp., Tokyo, Japan) with sampling frequency of 1.5 kHz. Echocardiography was performed using a Sonos 5500 (Hewlett Packard, Andover, MA).

Enzyme-Linked Immunosorbent Assay (ELISA)

Mouse hearts were isolated, washed, homogenized in ice-cold PBS, and centrifuged. The protein level in the supernatant was adjusted to 10 mg/ml by the BCA protein assay kit (Pierce, Rockford, IL), and subjected to ELISA using a VEGF ELISA kit (R&D Systems, Minneapolis, MN). Carrageenan (Sigma) and rat anti-mouse CD11b monoclonal antibody (Serotec, Oxford, UK) treatment was performed as previously reported.[14] Culture medium of mouse primary cardiomyocytes (2×10^5 cells) was changed daily. H9c2 myoblasts (5×10^3 cells) were differentiated to cardiomyocytes or myotubes. H9c2 cardiomyocytes were incubated with M-CSF and ATRA in the presence or absence of LY294002 (10 μmol/L) for indicated time periods with daily culture medium change. H9c2 myotubes were cultured with M-CSF for indicated time periods. All of the supernatants were assayed by ELISA.

RNA Isolation and Reverse Transcriptase-Polymerase Chain Reaction (RT-PCR)

Total RNA was isolated using RNAzol B reagent (Tel-Test, Friendswood, TX). Placenta total RNA was purchased from BD Biosciences. Quantitative RT-PCR for VEGF and conventional RT-PCR for M-CSF-R were performed as previously shown.[14]

Data Analysis

Data are presented as mean ± SD. Statistical analysis was performed using analysis of variance with Fisher's least significant difference test. P values <0.05 were considered as significant.

Results

M-CSF Increases Heart VEGF Production in Vivo

Previous studies have shown that M-CSF increased VEGF production in skeletal muscles, and the heart expresses VEGF. Therefore, we examined whether M-CSF increases heart VEGF production. Mice were treated with M-CSF, and then the cytoplasmic RNA in heart was assessed by quantitative RT-PCR. M-CSF significantly increased VEGF mRNA expression level in the hearts by 221% (Figure 1A). M-CSF receptor (M-CSF-R) mRNA expression was confirmed by conventional RT-PCR, and placenta-derived mRNA was used as a positive control (Figure 1B). To confirm VEGF at the protein level, M-CSF was injected into mice. The hearts were isolated, and ELISA for VEGF was performed. VEGF was detected in controls (Figure 1C). M-CSF significantly increased VEGF in the hearts by 21% (Figure 1C). Because M-CSF induces VEGF production *in vitro* from human monocytes,[29] we sought to clarify whether cardiomyocytes or the monocytes/macrophages in the heart produced VEGF after M-CSF treatment. Mice were treated with carra-

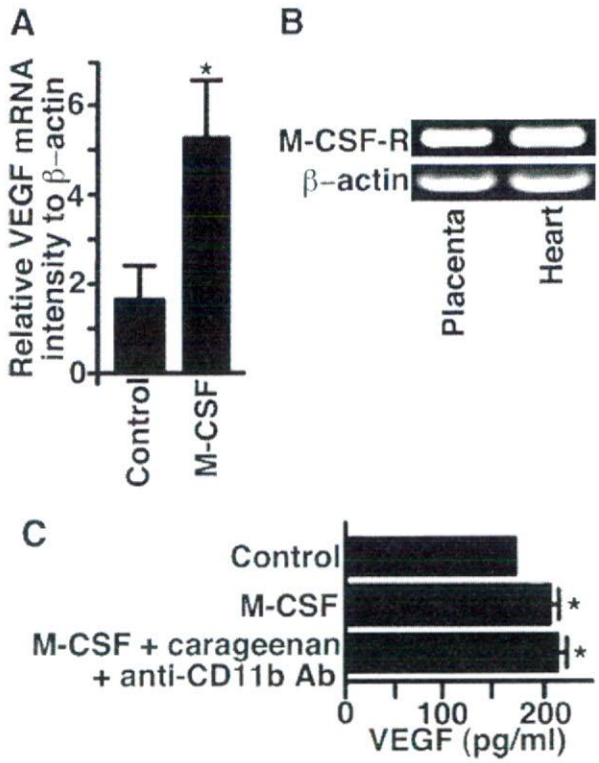

Figure 1. M-CSF increased heart VEGF production *in vivo*. Mice were injected intramuscularly with M-CSF (200 μg/kg) or PBS (control) for 3 consecutive days ($n = 5$ per group). **A:** Quantitative RT-PCR determined the VEGF mRNA expression. M-CSF treatment significantly increased the VEGF mRNA expression in hearts ($^*P < 0.05$). **B:** Conventional RT-PCR determined the M-CSF receptor (M-CSF-R) expression (top), and β-actin expression (bottom). **C:** The hearts were washed, homogenized in PBS, and centrifuged. ELISA determined the VEGF level in the supernatants containing 10 mg/ml protein. M-CSF significantly increased the VEGF level. M-CSF + carrageenan + anti-CD11b Ab indicates mice injected with carrageenin (1 mg) on days 1 and 4, with anti-CD11b monoclonal antibody (0.5 mg) on days 3 and 5, and with M-CSF on days 3, 4, and 5. On day 6, the hearts were isolated. This treatment did not affect the VEGF level ($^*P < 0.05$). Similar results were obtained from two independent experiments.

geenan and anti-CD11b monoclonal antibody to eliminate the monocytes/macrophages, as shown previously.[14] Macrophages were hardly observed in control mice hearts or in treated mice hearts (data not shown). The treatment did not affect M-CSF-induced VEGF production in the heart (Figure 1C).

M-CSF Increases VEGF Production by Cardiomyocytes in Vitro

To confirm the effect of M-CSF on heart VEGF production *in vitro*, mouse neonatal cardiomyocytes were isolated and stimulated with M-CSF. The culture medium was changed daily to maintain cell viability. Control cardiomyocytes produced VEGF, and M-CSF significantly increased the VEGF level on days 2 (by 10%) and 3 (by 31%) (Figure 2A). The M-CSF-R expression on cardiomyocytes was confirmed by fluorescence-activated cell sorting analysis (Figure 2B).

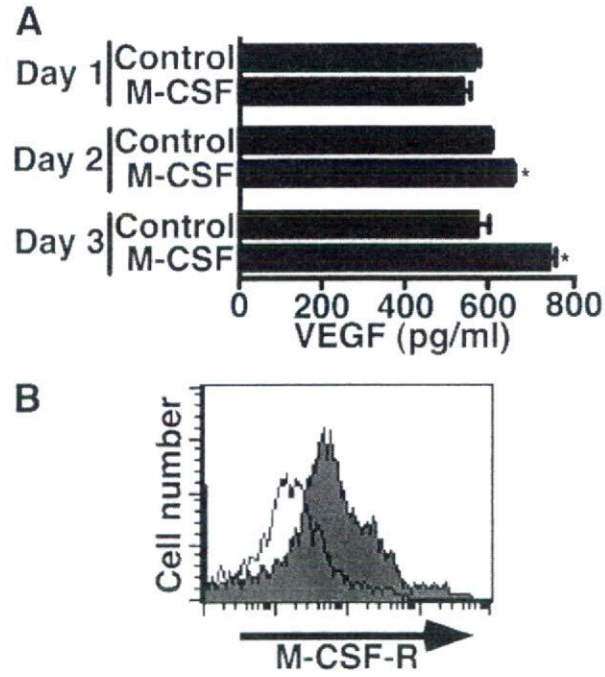

Figure 2. M-CSF enhanced heart VEGF production *in vitro*. **A:** Cultured cardiomyocytes from neonatal mice were stimulated with M-CSF (100 ng/ml) for the indicated time periods. Culture medium was changed daily, and the supernatants were subjected to ELISA. M-CSF significantly enhanced VEGF production on days 2 and 3 ($^*P < 0.01$). **B:** Cultured cardiomyocytes from neonatal mice expressed M-CSF-R. The shaded histogram indicates staining with M-CSF-R, and the blank histogram indicates background staining with control IgG. Similar results were obtained from two independent experiments.

M-CSF Increases VEGF Production from Differentiated H9c2 Cells

To investigate the effects of M-CSF on cardiomyocytes more precisely, rat H9c2 myoblast cells were differentiated to cardiomyocytes. H9c2 myoblasts differentiate to cardiomyocytes when they are cultured in DM with ATRA.[19] After differentiation, DM with ATRA was changed daily to maintain cell viability. VEGF was detected in supernatants from controls, and M-CSF increased H9c2 cardiomyocyte VEGF production on days 2 (by 10%) and 3 (by 20%) (Figure 3A). M-CSF increased skeletal muscle VEGF production.[14] H9c2 myoblasts cultured in the DM without ATRA for 11 days differentiate to H9c2 myotubes.[20] After differentiation, H9c2 myotubes were treated with M-CSF. H9c2 myotubes produced VEGF, and M-CSF significantly enhanced VEGF production on day 8 by 29% (Figure 3B).

M-CSF Protects Differentiated H9c2 Cells from H_2O_2-Induced Cell Death

Because M-CSF increased VEGF production from differentiated H9c2 cells, we investigated whether M-CSF increased the H9c2 cardiomyocyte cell number and found that it did not (Figure 4A). Similar results were obtained from the H9c2 myotubes (Figure 4A). M-CSF improves the survival of the mononuclear phagocyte lineage

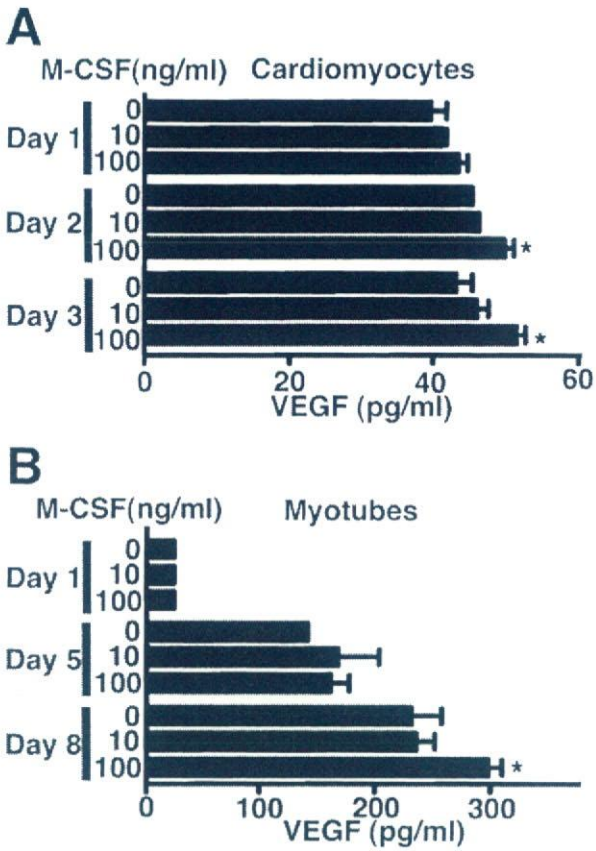

Figure 3. M-CSF increased VEGF production in differentiated H9c2 cells. **A:** H9c2 myoblasts cultured in DM (changed every 2 days) with daily supplementation of 10 nmol/L ATRA for 7 days were differentiated to H9c2 cardiomyocytes. The cells were stimulated with the indicated amount of M-CSF for indicated time periods. The culture medium was changed daily, and ELISA determined the VEGF level in the supernatant. M-CSF (100 ng/ml) increased VEGF production on days 2 and 3 ($^*P < 0.05$). **B:** H9c2 myoblasts cultured in the same DM for 11 days were differentiated to H9c2 myotubes. Then the cells were stimulated with the indicated amount of M-CSF for the indicated time periods without medium change. M-CSF (100 ng/ml) significantly increased VEGF production on day 8 ($^*P < 0.03$). Similar results were obtained from three independent experiments.

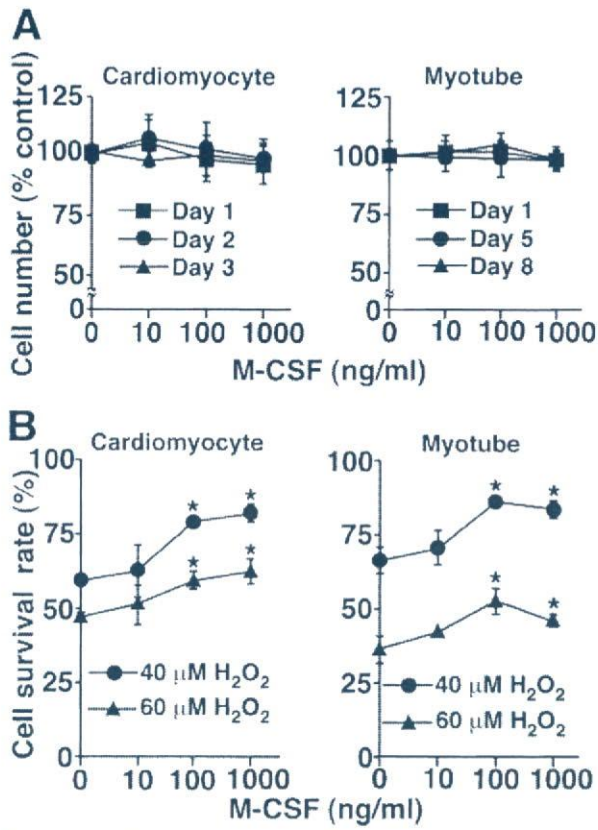

Figure 4. M-CSF protects differentiated H9c2 cells from H_2O_2-induced cell death. **A:** H9c2 cardiomyocytes were cultured with the indicated amount of M-CSF and ATRA for the indicated time periods, and the culture medium was changed daily. H9c2 myotubes were cultured with the indicated amount of M-CSF for the indicated time periods. WST assay determined the cell number. **B:** H9c2 cardiomyocytes or H9c2 myotubes were cultured with the indicated amount of M-CSF for 24 hours and then stimulated with H_2O_2 (40 or 60 μmol/L) for 8 hours. The culture medium of H9c2 cardiomyocytes was supplemented with ATRA. WST assay determined the cell viability. M-CSF (100 and 1000 ng/ml) significantly protected the cells from H_2O_2-induced cell death ($^*P < 0.03$). Similar results were obtained from three independent experiments.

cells.[11] Therefore, the cell survival effect of M-CSF on differentiated H9c2 cells from cytotoxic H_2O_2 exposure was examined. H9c2 cardiomyocytes were incubated with M-CSF and then exposed to H_2O_2. M-CSF significantly protected H9c2 cardiomyocytes from H_2O_2-induced cell death (Figure 4B). Similar results were obtained from H9c2 myotubes (Figure 4B).

M-CSF Activates ERK and Akt Signaling Pathways and Increases Bcl-xL Expression in Differentiated H9c2 Cells

The cell signaling pathways of M-CSF in cardiomyocytes and H9c2 myotubes have not been investigated. To elucidate molecular mechanisms of the M-CSF-induced cell survival, differentiated H9c2 cells were treated with M-CSF and then activation of ERK, Akt, and Jak-STAT signaling pathways was investigated. Western blot analysis showed two forms of M-CSF-R in differentiated H9c2 cells (Figure 5, A and C).[30] In H9c2 cardiomyocytes, M-CSF induced ERK activation, as indicated by its protein phosphorylation, whereas the protein levels of the total ERK in cell lysates were not different (Figure 5A). M-CSF activated the Akt, but M-CSF did not activate Jak1, Stat1, or Stat3 (Figure 5A). ERK activation protects cardiomyocytes from cell death by up-regulating the anti-apoptotic protein Bcl-xL and inactivating the apoptotic protein Bad by its phosphorylation at Ser112.[31,32] Akt activation improves cardiomyocyte survival, but the main downstream signaling pathways of Akt for cardiomyocytes survival has not been clarified.[33] To clarify the target molecules of ERK in H9c2 cardiomyocytes, Bcl-xL expression was examined. Bcl-xL was detected in cells without M-CSF stimulation (Figure 5B). M-CSF up-regulated Bcl-xL expression, which peaked at 24 and 48 hours (Figure 5B). M-CSF did not phosphorylate Bad at Ser112 (Figure 5B). These results suggest M-CSF protected H9c2 cardiomyocytes by activating Akt and up-regulating Bcl-xL expression through ERK activation. In H9c2 myotubes, M-CSF activated ERK and Akt but did not activate Jak1 or Stat3

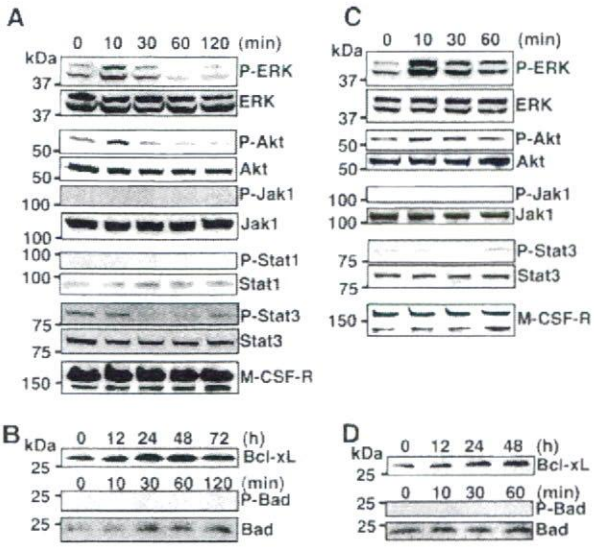

Figure 5. M-CSF activated ERK, Akt, and up-regulated Bcl-xL expression in differentiated H9c2 cells. H9c2 cardiomyocytes (**A** and **B**) or H9c2 myotubes (**C** and **D**) were stimulated with M-CSF (100 ng/ml) for the indicated time periods, and then the cell lysates were blotted with antibodies specific for the activated form of ERK (phospho-ERK), Akt (phospho-Akt), Jak1 (phospho-Jak1), Stat1 (phospho-Stat1), Stat3 (phospho-Stat3), or phosphorylated Bad (phospho-Bad). The membranes were reblotted with antibodies to total ERK, Akt, Jak1, Stat1, Stat3, or Bad, respectively. Expression of M-CSF-R or Bcl-xL was confirmed by blotting the membrane with specific antibodies. Similar results were obtained from three independent experiments.

(Figure 5C). M-CSF gradually up-regulated Bcl-xL expression until 48 hours (Figure 5D) but did not phosphorylate Bad at Ser112 (Figure 5D).

The Role of M-CSF-Induced Akt and ERK Activation in VEGF Production and Cell Survival in Differentiated H9c2 Cells

M-CSF increases VEGF production through Akt activation in skeletal muscles. To determine the role of Akt activation in H9c2 cardiomyocytes VEGF production, H9c2 cardiomyocytes were treated with Akt-specific inhibitor LY294002, and the culture supernatant was assayed by ELISA. LY294002 and M-CSF treatment for 2 days significantly impaired VEGF production in H9c2 cardiomyocytes (Figure 6A). LY294002 and M-CSF treatment for 3 days further decreased VEGF production, and the VEGF level became less than the detection level (Figure 6A). To determine the role of ERK and Akt activation after M-CSF treatment in differentiated H9c2 cell survival, differentiated H9c2 cells were treated with LY294002 or the ERK-specific inhibitor PD98059. PD98059 inhibited ERK activation and LY294002 inhibited Akt activation in H9c2 cardiomyocytes (Figure 6B). Similar results were obtained from H9c2 myotubes (data not shown). PD98059 enhanced H_2O_2-induced cell death of H9c2 cardiomyocytes (Figure 6C). The protective effect of M-CSF was impaired by PD98059; however, M-CSF significantly protected H9c2 cardiomyocytes from cell death (Figure 6C). A similar result was obtained from LY294002 in H9c2 cardiomyocytes (Figure 6C). In H9c2 myotubes, PD 98059 enhanced H_2O_2-induced cell death, and PD98059

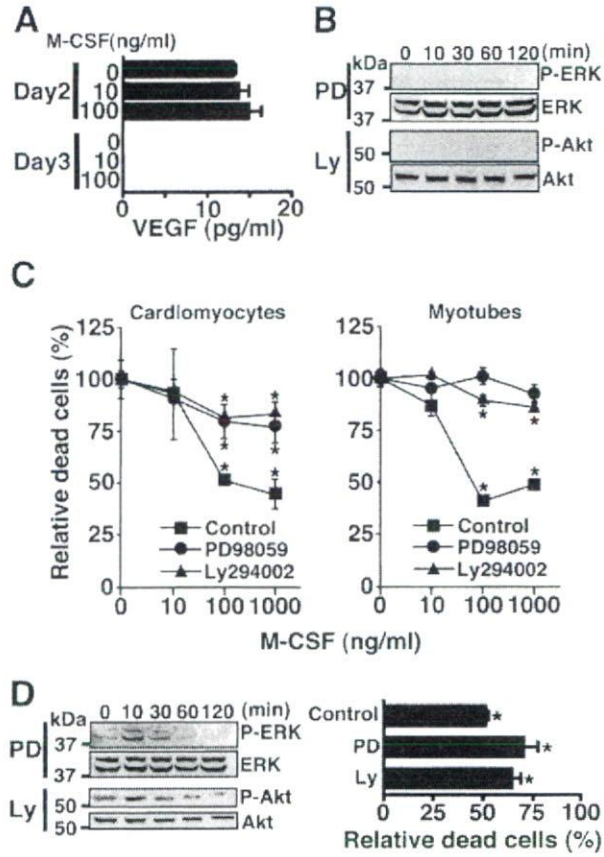

Figure 6. The role of M-CSF-induced Akt and ERK activation in VEGF production and cell protection in differentiated H9c2 cells. **A:** H9c2 cardiomyocytes were cultured with M-CSF and 10 μmol/L LY294002 for the indicated time periods. The culture medium was changed daily and ELISA determined the VEGF level. **B:** H9c2 cardiomyocytes were incubated with 30 μmol/L PD98059 (PD) or 10 μmol/L LY294002 (Ly) for 30 minutes, then stimulated with M-CSF (100 ng/ml) and inhibitors, and analyzed as described in Figure 5. **C:** Differentiated H9c2 cells were stimulated with indicated amount of M-CSF with PD98059 (30 μmol/L) or LY294002 (10 μmol/L) for 24 hours. Then the cells were stimulated with H_2O_2 (40 μmol/L) for 8 hours, and WST assay determined the dead cells. M-CSF (0 ng/ml) in each group is considered as 100%, and relative cell death rates in each group are shown. $^*P < 0.03$ compared with 0 ng/ml M-CSF in each group. Similar results were obtained from three independent experiments. **D:** H9c2 cardiomyocytes were incubated with reduced concentrations of PD98059 (6 μmol/L) or LY294002 (2 μmol/L). Left: H9c2 cardiomyocytes were treated with PD98059 or LY294002 for 30 minutes, stimulated with M-CSF (100 ng/ml) and inhibitors, and then analyzed as described in Figure 5. Right: H9c2 cardiomyocytes were treated with PD98059, LY294002, or without inhibitors (control) with (100 ng/ml) or without (0 ng/ml) M-CSF for 24 hours. Then the cells were stimulated with H_2O_2 (40 μmol/L) for 8 hours, and dead cells were assessed by WST assay. In each inhibitor group, dead cells at 0 ng/ml M-CSF are considered as 100%, and relative cell death rates at 100 to 0 ng/ml M-CSF in each inhibitor group are shown. $^*P < 0.02$ compared with 0 ng/ml M-CSF in each group.

abolished the protective effect of M-CSF (Figure 6C). LY294002 enhanced H_2O_2-induced cell death in H9c2 myotubes; however, M-CSF significantly protected H9c2 myotubes from cell death (Figure 6C). Moreover, a dose-response experiment of PD98059 or LY294002 was performed to observe ERK or Akt phosphorylation and cellular survival of H9c2 cardiomyocytes (Figure 6D). Similar results were obtained from H9c2 myotubes (data not shown). VEGF protected myogenic cells from cell death.[34] To confirm whether the cell survival effect of M-CSF de-

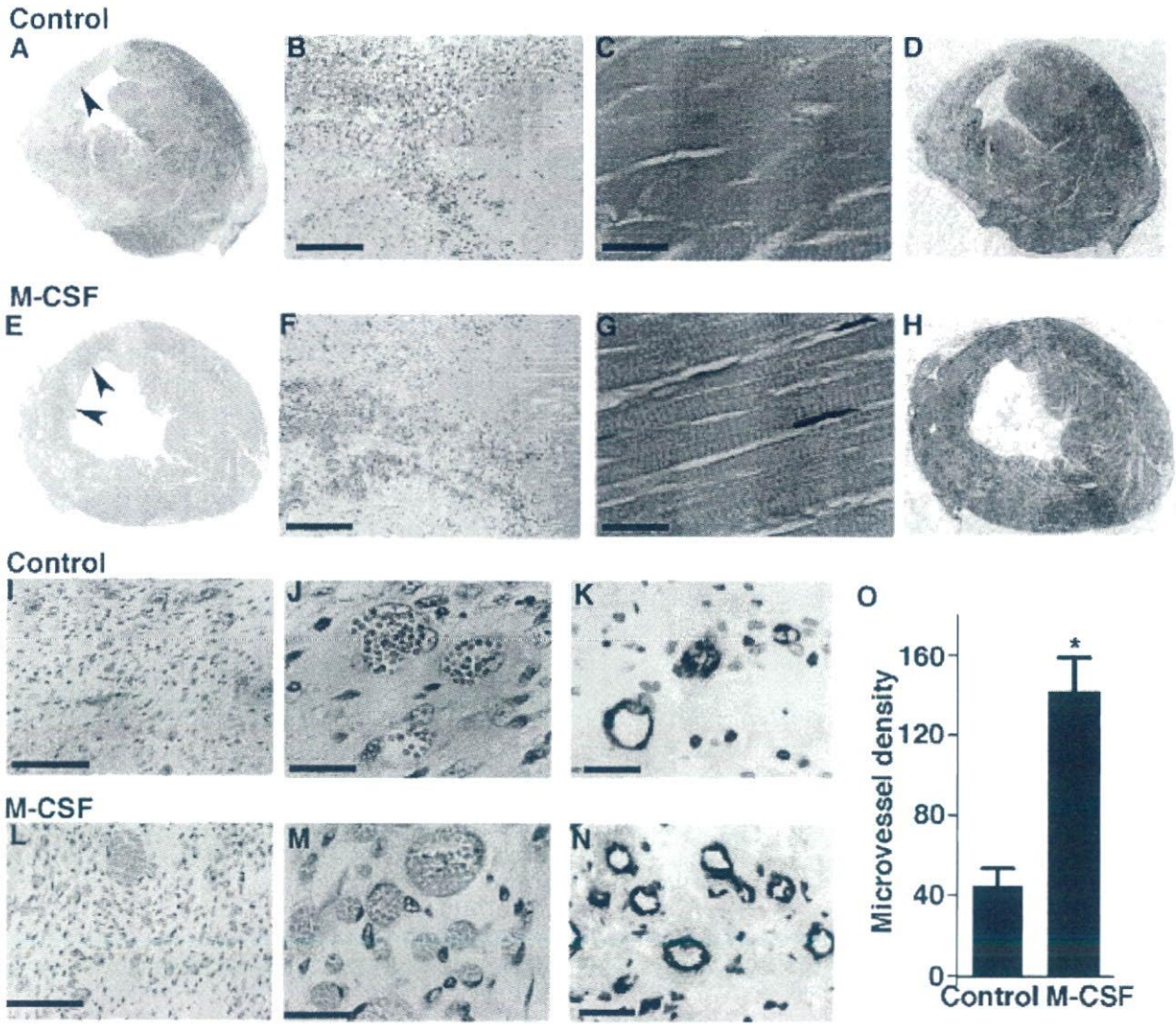

Figure 7. M-CSF promotes angiogenesis in goat heart after myocardial infarction. The goat left anterior descending coronary artery was permanently ligated, and the goats were sacrificed on day 14. M-CSF indicates goats intravenously injected with M-CSF shortly after the coronary artery ligation daily until day 13. Controls were injected with saline. Paraffin sections were stained with H&E (**A–C**, **E–G**, **I**, **J**, **L**, and **M**), Masson's elastic stain (**D** and **H**), and anti-factor VIII-related antigen antibody (**K** and **N**). **A** and **E:** Left anterior descending coronary artery ligation induced myocardial infarction. **Arrowheads** indicate cardiomyocytes in ischemic lesions. (**B**, **C**, **F**, and **G**) Microscopic observations indicated the cardiomyocytes in the ischemic lesions were dead. **D** and **H:** The green staining indicates fibrosis or scars in hearts. **I**, **J**, **L**, and **M:** The microvessels in ischemic lesions. **K** and **N:** The microvessels in ischemic lesions were immunohistochemically stained with anti-factor VIII-related antigen antibody. **O:** M-CSF significantly increased microvessel density in ischemic lesions ($^*P < 0.01$, $n = 3$ per group). The images represent one of three goats in each group. Scale bars: 200 μm (**B** and **F**); 20 μm (**C**, **G**, **J**, **K**, **M**, and **N**); 100 μm (**I** and **L**).

pends on VEGF, H9c2 cardiomyocytes and myotubes were cultured with an anti-VEGF antibody and M-CSF. Incubation with anti-VEGF antibody did not impair the cell protective effect of M-CSF from H_2O_2 stimulation suggesting that the effect of M-CSF was not VEGF-dependent (data not shown).

M-CSF Promotes Angiogenesis in Goat Ischemic Heart after Permanent Coronary Artery Ligation

M-CSF treatment elevated systemic VEGF level in mice from a nondetectable level to potentially therapeutic levels.[14,15] The cell protective and angiogenic effects of M-CSF *in vivo* were examined using goats as a large animal model for myocardial infarction. Large animal models are necessary for evaluating growth factor-induced therapeutic angiogenesis,[3] and we have used goats for developing artificial heart devices.[27] We induced myocardial infarction by permanent left anterior descending coronary artery ligation. The coronary artery ligation resulted in LV infarction (Figure 7, A, D, E, and H). Macroscopically, M-CSF seemed to promote cardiomyocyte cell survival in ischemic lesions in comparison to the controls (Figure 7, A and E; arrowheads). Microscopy indicated that cardiomyocytes in ischemic lesions were dead cells in the controls (Figure 7, B and C). At low magnification, M-CSF seemed to protect cardiomyocytes from cell death in ischemic lesions (Figure 7F). However,

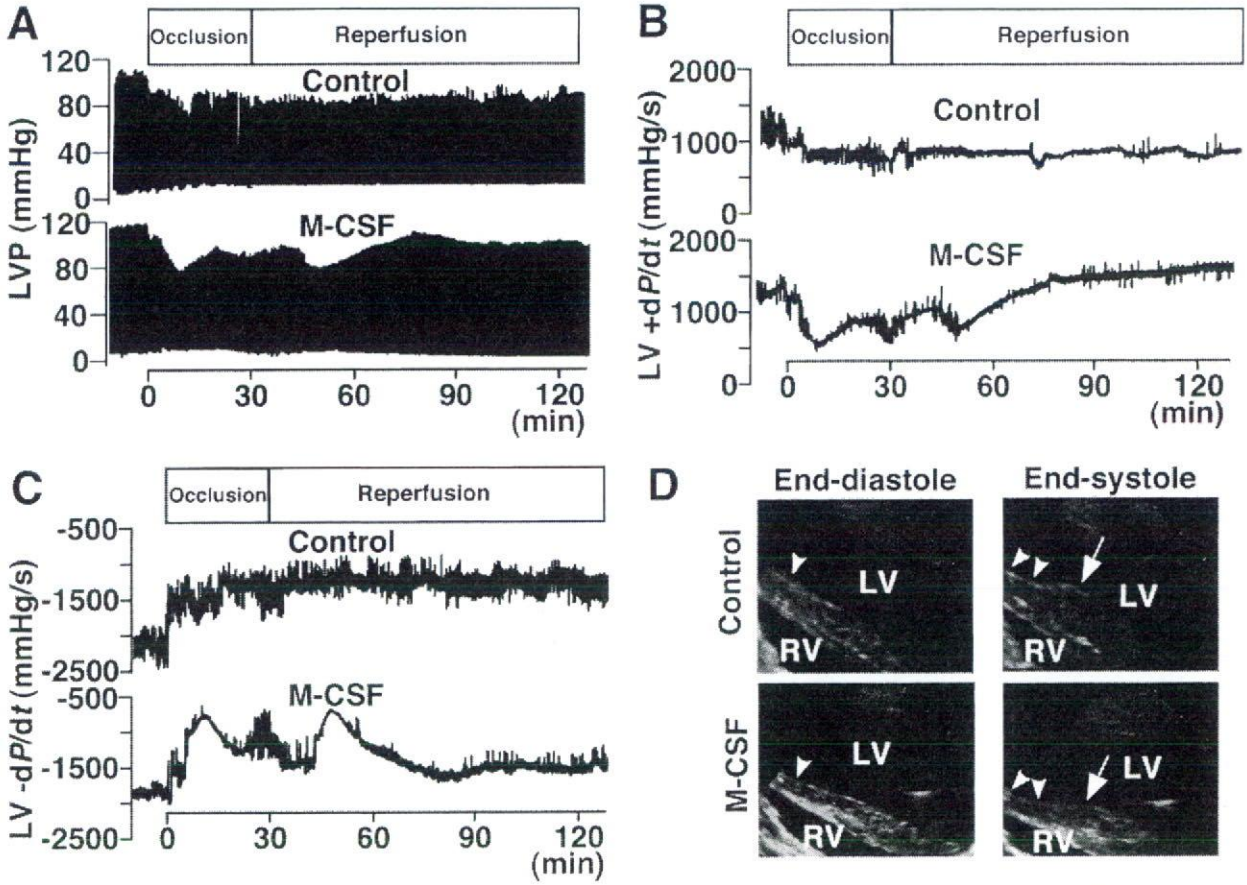

Figure 8. M-CSF pretreatment improved cardiac function after ischemic injury. M-CSF indicates goats intravenously injected with M-CSF daily for 3 days, whereas the control indicates goats injected with saline. The goat left anterior descending coronary artery was occluded for 30 minutes and then reperfused. **A–C:** Hemodynamic parameters before and during 30 minutes of left anterior descending coronary artery occlusion followed by 90 minutes of reperfusion are shown. Representative LVP records (**A**), representative positive dP/dt (**B**), and representative negative dP/dt (**C**) of control and M-CSF-treated goats. LVEDP, positive and negative dP/dt recovered in M-CSF-treated goats after reperfusion. **D: Arrowheads** indicate infarct areas. Compare **arrows**, which indicate wall contraction of nonischemic area at end systole, to **arrowheads**. In the infarct area, echocardiography shows dyskinetic wall movement in controls, whereas akinetic wall movement is shown in M-CSF-treated goats. Data are representative of three goats in each group.

at high magnification, most of the cardiomyocytes were dead (Figure 7G). Microvessels were observed in the ischemic lesions of control goats (Figure 7, I and J), and M-CSF treatment increased the number of microvessels (Figure 7, L and M). To confirm the microvessel density, we immunohistochemically stained goat hearts with anti-factor VIII-related antigen antibody (Figure 8, K and N).[23,24] M-CSF significantly increased microvessel density in ischemic lesions by 226% (Figure 7O). These results suggest that M-CSF promoted angiogenesis and induced collateral blood vessels in the ischemic heart. The infarct area quantification showed no significant difference between control and M-CSF-treated goats (controls, 30.4 ± 5.2%; M-CSF, 24.3 ± 2.1%). The residual presence of nuclei and cross striations in dead cardiomyocytes in ischemic lesions by M-CSF treatment (Figure 7G) suggests that the cardiomyocytes survived longer than control cardiomyocytes (Figure 7, C and G), but M-CSF-induced new vessels could not reach cardiomyocytes in ischemic lesions before their death.

M-CSF Pretreatment Improved Cardiac Function after Ischemic Injury Induced by Coronary Artery Occlusion-Reperfusion

Erythropoietin treatment did not change the infarct size, but it improved cardiac function in the rat coronary artery occlusion-reperfusion model.[5] Pretreatment with stem cell factor and G-CSF improved cardiac function after myocardial infarction.[7] To confirm further the effects of M-CSF in myocardial infarction, goats were pretreated with M-CSF for 3 days, and then myocardial infarction was induced by 30-minute left anterior descending coronary artery occlusion followed by reperfusion.[5,35] Cardiac function was assessed by measuring hemodynamic parameters using catheterization analysis and examining echocardiography. Echocardiographic examination showed no significant differences in basal findings in cardiac function in both groups. Catheterization analysis showed the LV pressure (LVP) records of control and M-CSF-treated goats (Figure 8A). LV end diastolic pressure

(LVEDP), which can influence overall cardiac function,[4] increased after the left anterior descending coronary artery occlusion in both groups. In controls, the LVEDP did not recover after reperfusion, but in M-CSF-treated goats, the LVEDP gradually recovered after reperfusion (Figure 8A), and at 90 minutes after the reperfusion, the LVEDP of M-CSF treated goats was significantly better than that of control goats (controls, 10.62 ± 0.98 mmHg; M-CSF, 7.61 ± 0.83 mmHg; $P < 0.02$). Positive and negative dP/dt are measures of overall cardiac contractility and relaxation, respectively.[4] Positive dP/dt decreased after the left anterior descending coronary artery occlusion both in control and M-CSF-treated goats (Figure 8B). After reperfusion, positive dP/dt did not recover in control goats (Figure 8B). In M-CSF treated goats, positive dP/dt gradually recovered after reperfusion and finally reached similar dP/dt levels before the occlusion (Figure 8B). At 90 minutes after the reperfusion, the positive dP/dt of M-CSF-treated goats was significantly better than that of control goats (controls, 886 ± 103 mmHg; M-CSF, 1506 ± 125 mmHg; $P < 0.01$). Moreover, recovery of negative dP/dt after left anterior descending coronary artery occlusion-reperfusion was observed only in M-CSF-treated goats (Figure 8C). At 90 minutes after the reperfusion, the negative dP/dt of M-CSF-treated goats was significantly better than that of control goats (controls, −1342 ± 92 mmHg; M-CSF, −1570 ± 108 mmHg; $P < 0.05$). Echocardiographic examination showed a paradoxical LV wall movement area indicated as a dyskinetic area after left anterior descending coronary artery occlusion in control goats (Figure 8D). In M-CSF-treated goats, echocardiography showed a LV wall movement arrest area indicated as an akinetic area after left anterior descending coronary artery occlusion, and a dyskinetic area could not be found (Figure 8D). In control hearts, the nonischemic wall contractions at end systole were enhanced. This suggested substitutive wall movement for the dyskinetic area to keep cardiac output (Figure 8D). These echocardiographic findings suggest improvement of LV wall movement in M-CSF-treated goats during left anterior descending coronary artery occlusion-reperfusion. The LV ejection fraction (LVEF) was evaluated by echocardiography, but LVEF did not significantly change between before and after the occlusion; therefore, LVEF between controls and M-CSF-treated ones were not compared. Recovery of LVEDP, positive and negative d*P*/d*t* after reperfusion, and improvement of LV wall movement during the left anterior descending coronary artery occlusion-reperfusion suggest M-CSF pretreatment improved cardiac function after ischemic injury

Discussion

In this study, M-CSF increased VEGF production in hearts both *in vivo* and *in vitro*. *In vitro*, M-CSF increased VEGF production through Akt activation. Moreover, M-CSF directly protected cardiomyocytes from cell death by activating Akt and ERK resulting in up-regulation of the downstream anti-apoptotic protein Bcl-xL. M-CSF-R expression in the heart was shown both *in vivo* and *in vitro*, and these results suggest that the expression is functional. Similar cell-protective effects of M-CSF on H9c2 myotubes were shown. *In vivo*, M-CSF treatment after the onset of myocardial infarction promoted angiogenesis in the ischemic heart, suggesting development of collateral blood vessels. Furthermore, M-CSF pretreatment in the goat myocardial infarction model improves cardiac function, as indicated by improvement of LVEDP, positive and negative dP/dt, and LV wall movements.

Recent studies indicate intramyocardial transfer of plasmid or adenoviral DNA-encoding human VEGF has favorable effects in myocardial infarction animal models and in patients with coronary artery diseases.[1,2,36] Similar to these VEGF transfer strategies, M-CSF directly up-regulated VEGF production in cardiomyocytes. In addition, M-CSF significantly induced an increase in plasma VEGF in mice to therapeutic levels that induced therapeutic angiogenesis.[14,35] Therapeutic plasmid gene delivery to a target organ is difficult and often temporary. However, M-CSF treatment was easily achieved by peripheral intravenous or intramuscular injection. These data indicate a therapeutic potential of M-CSF in ischemic heart diseases. Basic fibroblast growth factor and hepatocyte growth factor have also been applied to therapeutic angiogenesis.[37] We treated mice with M-CSF and examined basic fibroblast growth factor and hepatocyte growth factor mRNA levels by quantitative RT-PCR. M-CSF did not increase basic fibroblast growth factor or hepatocyte growth factor mRNA levels in the heart (data not shown). We also examined plasma G-CSF level after M-CSF treatment in mice by ELISA. M-CSF did not increase plasma G-CSF level. However, there is still a possibility that M-CSF induces other factors that are responsible for the effects shown in this article.

Very recently, M-CSF was reported to accelerate infarct repair and attenuate LV dysfunction in rats.[35] However, these authors did not investigate VEGF induction or the cardioprotective effects of M-CSF and did not use a large animal model. In the present study, in the M-CSF-treated group, we observed an increase in microvessel density, increased presence of dead cardiomyocytes, and decreased presence of granuloma in ischemic lesions. The increased presence of dead cardiomyocytes in ischemic lesions and improvement of cardiac function after ischemia in M-CSF-treated goats suggest a longer survival of cardiomyocytes in M-CSF-treated goats than in the controls. This finding and the decreased presence of granuloma suggest that M-CSF reduced the progression rate of ischemic injury in ischemic hearts *in vivo*.

In human monocytes, LY294002 suppressed M-CSF-induced ERK activation.[38] This mechanism was explained as M-CSF stimulation-induced reactive oxygen species, which activated ERK. The addition of Akt inhibitor prevented reactive oxygen species production and thus suppressed ERK activation in M-CSF-stimulated monocytes.[38] In murine myeloid cell line FDC-P1, LY294002 suppressed M-CSF-induced ERK activation, but it was not significant.[39] In H9c2 cardiomyocytes, LY294002 seemed to impair ERK activation in part. To suggest the involvement of Akt in M-CSF-induced ERK

activation in cardiomyocytes, we may have to use other Akt-inhibiting methods, as this time we could not reach a clear conclusion. For VEGF production, PD98059 treatment for 1 day did not affect M-CSF-induced VEGF production in differentiated H9c2 cells, whereas LY294002 treatment impaired M-CSF-induced VEGF production, suggesting M-CSF-induced VEGF production in differentiated H9c2 cells were Akt-dependent. This is the first report that suggested the presence of signal transduction pathways in cardiomyocytes in response to M-CSF. Further experiments are required for pursuing the M-CSF-induced intracellular signaling pathways in cardiomyocytes or in myotubes.

Goat hearts have a left coronary artery-dominant blood supply.[40] The goat coronary artery anatomy was remarkably regular, and coronary artery collaterals could not be demonstrated,[40] indicating frailty after heart ischemic injury. For the left anterior descending coronary artery occlusion-reperfusion model, the goat left anterior descending coronary artery was ligated at a point ~40% from the beginning of the left coronary artery to the apex, but LVEF decrease could not be detected by echocardiography. Occlusion of a more proximal site of goat left anterior descending coronary artery has been reported to be invariably fatal,[40] and our preliminary experiments with a more proximal left anterior descending coronary artery ligation supported this finding. Therefore, using goats, LVEF after myocardial infarction could not be evaluated. We were not able to assess plasma VEGF and the involvement of bone marrow-derived cells in the goat model because the appropriate reagents are not commercially available. We could not find a staining method specific for cardiomyocyte viability in goat hearts. Infarct area quantification suggested a trend that M-CSF might decrease infarct area. However, infarct area quantification showed no significant difference in control and M-CSF-treated goat hearts. Further investigation is required to clarify the roles and mechanisms of M-CSF in ischemic diseases using other species and other M-CSF treatment protocols.

The cell-protective and VEGF-inducing effects of M-CSF both in cardiomyocytes and myotubes were shown, and the effects were confirmed by improvement of cardiac function and activated angiogenesis in goat ischemic hearts. M-CSF is already in use clinically, and data from patients such as side effects are accumulating. Moreover, M-CSF administration is easily performed with minimal invasiveness in human patients. In this study, we showed the potential benefits of M-CSF treatment and its new mechanisms in ischemic heart diseases.

Acknowledgments

We thank Peter Baluk, Hiroya Hashizume, Hiroshi Kubo, and Katsutoshi Nakayama for helpful comments on the manuscript; and Amy Ni and Shannon Freeman for correcting the manuscript.

References

1. Yoon YS, Johnson IA, Park JS, Diaz L, Losordo DW: Therapeutic myocardial angiogenesis with vascular endothelial growth factors. Mol Cell Biochem 2004, 264:63–74
2. Kastrup J, Jorgensen E, Ruck A, Tagil K, Glogar D, Ruzyllo W, Botker HE, Dudek D, Drvota V, Hesse B, Thuesen L, Blomberg P, Gyongyosi M, Sylven C: Direct intramyocardial plasmid vascular endothelial growth factor-A165 gene therapy in patients with stable severe angina pectoris A randomized double-blind placebo-controlled study: the Euroinject One trial. J Am Coll Cardiol 2005, 45:982–988
3. Markkanen JE, Rissanen TT, Kivela A, Yla-Herttuala S: Growth factor-induced therapeutic angiogenesis and arteriogenesis in the heart-gene therapy. Cardiovasc Res 2005, 65:656–664
4. Parsa CJ, Matsumoto A, Kim J, Riel RU, Pascal LS, Walton GB, Thompson RB, Petrofski JA, Annex BH, Stamler JS, Koch WJ: A novel protective effect of erythropoietin in the infarcted heart. J Clin Invest 2003, 112:999–1007
5. Calvillo L, Latini R, Kajstura J, Leri A, Anversa P, Ghezzi P, Salio M, Cerami A, Brines M: Recombinant human erythropoietin protects the myocardium from ischemia-reperfusion injury and promotes beneficial remodeling. Proc Natl Acad Sci USA 2003, 100:4802–4806
6. Harada M, Qin Y, Takano H, Minamino T, Zou Y, Toko H, Ohtsuka M, Matsuura K, Sano M, Nishi J, Iwanaga K, Akazawa H, Kunieda T, Zhu W, Hasegawa H, Kunisada K, Nagai T, Nakaya H, Yamauchi-Takihara K, Komuro I: G-CSF prevents cardiac remodeling after myocardial infarction by activating the Jak-Stat pathway in cardiomyocytes. Nat Med 2005, 11:305–311
7. Orlic D, Kajstura J, Chimenti S, Limana F, Jakoniuk I, Quaini F, Nadal-Ginard B, Bodine DM, Leri A, Anversa P: Mobilized bone marrow cells repair the infarcted heart, improving function and survival. Proc Natl Acad Sci USA 2001, 98:10344–10349
8. Miki T, Miura T, Nishino Y, Yano T, Sakamoto J, Nakamura Y, Ichikawa Y, Ikeda Y, Kobayashi H, Ura N, Shimamoto K: Granulocyte colony stimulating factor/macrophage colony stimulating factor improves postinfarct ventricular function by suppression of border zone remodelling in rats. Clin Exp Pharmacol Physiol 2004, 31:873–882
9. Ohno R, Miyawaki S, Hatake K, Kuriyama K, Saito K, Kanamaru A, Kobayashi T, Kodera Y, Nishikawa K, Matsuda S, Yamada O, Omoto E, Takeyama H, Tsukuda K, Asou N, Tanimoto M, Shiozaki H, Tomonaga M, Masaoka T, Miura Y, Takaku F, Ohashi Y, Motoyoshi K: Human urinary macrophage colony-stimulating factor reduces the incidence and duration of febrile neutropenia and shortens the period required to finish three courses of intensive consolidation therapy in acute myeloid leukemia: a double-blind controlled study. J Clin Oncol 1997, 15:2954–2965
10. Kawakami Y, Nagai N, Ohama K, Zeki K, Yoshida Y, Kuroda E, Yamashita U: Macrophage-colony stimulating factor inhibits the growth of human ovarian cancer cells in vitro. Eur J Cancer 2000, 36:1991–1997
11. Stanley ER, Berg KL, Einstein DB, Lee PS, Pixley FJ, Wang Y, Yeung YG: Biology and action of colony-stimulating factor-1. Mol Reprod Dev 1997, 46:4–10
12. Giordano FJ, Gerber HP, Williams SP, VanBruggen N, Bunting S, Ruiz-Lozano P, Gu Y, Nath AK, Huang Y, Hickey R, Dalton N, Peterson KL, Ross Jr J, Chien KR, Ferrara N: A cardiac myocyte vascular endothelial growth factor paracrine pathway is required to maintain cardiac function. Proc Natl Acad Sci USA 2001, 98:5780–5785
13. Maharaj AS, Saint-Geniez M, Maldonado AE, D'Amore PA: Vascular endothelial growth factor localization in the adult. Am J Pathol 2006, 168:639–648
14. Okazaki T, Ebihara S, Takahashi H, Asada M, Kanda A, Sasaki H: Macrophage colony-stimulating factor induces vascular endothelial growth factor production in skeletal muscle and promotes tumor angiogenesis. J Immunol 2005, 174:7531–7538
15. Kalka C, Masuda H, Takahashi T, Gordon R, Tepper O, Gravereaux E, Pieczek A, Iwaguro H, Hayashi SI, Isner JM, Asahara T: Vascular endothelial growth factor$_{165}$ gene transfer augments circulating endothelial progenitor cells in human subjects. Circ Res 2000, 86:1198–1202
16. Kallies A, Rosenbauer F, Scheller M, Knobeloch KP, Horak I: Accumulation of c-Cbl and rapid termination of colony-stimulating factor 1 receptor signaling in interferon consensus sequence bind-

ing protein-deficient bone marrow-derived macrophages. Blood 2002, 99:3213–3219
17. Novak U, Harpur AG, Paradiso L, Kanagasundaram V, Jaworowski A, Wilks AF, Hamilton JA: Colony-stimulating factor 1-induced STAT1 and STAT3 activation is accompanied by phosphorylation of Tyk2 in macrophages and Tyk2 and JAK1 in fibroblasts. Blood 1995, 86:2948–2956
18. Kelley TW, Graham MM, Doseff AI, Pomerantz RW, Lau SM, Ostrowski MC, Franke TF, Marsh CB: Macrophage colony-stimulating factor promotes cell survival through Akt/protein kinase B. J Biol Chem 1999, 274:26393–26398
19. Menard C, Pupier S, Mornet D, Kitzmann M, Nargeot J, Lory P: Modulation of L-type calcium channel expression during retinoic acid-induced differentiation of H9C2 cardiac cells. J Biol Chem 1999, 274:29063–29070
20. van den Eijnde SM, van den Hoff MJ, Reutelingsperger CP, van Heerde WL, Henfling ME, Vermeij-Keers C, Schutte B, Borgers M, Ramaekers FC: Transient expression of phosphatidylserine at cell-cell contact areas is required for myotube formation. J Cell Sci 2001, 114:3631–3642
21. Kang YJ, Zhou ZX, Wang GW, Buridi A, Klein JB: Suppression by metallothionein of doxorubicin-induced cardiomyocyte apoptosis through inhibition of p38 mitogen-activated protein kinases. J Biol Chem 2000, 275:13690–13698
22. Okazaki T, Sakon S, Sasazuki T, Sakurai H, Doi T, Yagita H, Okumura K, Nakano H: Phosphorylation of serine 276 is essential for p65 NF-κB subunit-dependent cellular responses. Biochem Biophys Res Commun 2003, 300:807–812
23. Seno H, Oshima M, Ishikawa TO, Oshima H, Takaku K, Chiba T, Narumiya S, Taketo MM: Cyclooxygenase 2- and prostaglandin E_2 receptor EP_2-dependent angiogenesis in $Apc^{\Delta 716}$ mouse intestinal polyps. Cancer Res 2002, 62:506–511
24. Bildfell RJ, Valentine BA, Whitney KM: Cutaneous vasoproliferative lesions in goats. Vet Pathol 2002, 39:273–277
25. Ebihara S, Guibinga GH, Gilbert R, Nalbantoglu J, Massie B, Karpati G, Petrof BJ: Differential effects of dystrophin and utrophin gene transfer in immunocompetent muscular dystrophy (mdx) mice. Physiol Genomics 2000, 3:133–144
26. Sakon S, Xue X, Takekawa M, Sasazuki T, Okazaki T, Kojima Y, Piao JH, Yagita H, Okumura K, Doi T, Nakano H: NF-κB inhibits TNF-induced accumulation of ROS that mediate prolonged MAPK activation and necrotic cell death. EMBO J 2003, 22:3898–3909
27. Wang Q, Yambe T, Shiraishi Y, Duan X, Nitta S, Tabayashi K, Umezu M: An artificial myocardium assist system: electrohydraulic ventricular actuation improves myocardial tissue perfusion in goats. Artif Organs 2004, 28:853–857
28. Kim WG, Cho SR, Sung SH, Park HJ: A chronic heart failure model by coronary artery ligation in the goat. Int J Artif Organs 2003, 26:929–934
29. Eubank TD, Galloway M, Montague CM, Waldman WJ, Marsh CB: M-CSF induces vascular endothelial growth factor production and angiogenic activity from human monocytes. J Immunol 2003, 171:2637–2643
30. Ide H, Seligson DB, Memarzadeh S, Xin L, Horvath S, Dubey P, Flick MB, Kacinski BM, Palotie A, Witte ON: Expression of colony-stimulating factor 1 receptor during prostate development and prostate cancer progression. Proc Natl Acad Sci USA 2002, 99:14404–14409
31. Baines CP, Molkentin JD: STRESS signaling pathways that modulate cardiac myocyte apoptosis. J Mol Cell Cardiol 2005, 38:47–62
32. Valks DM, Cook SA, Pham FH, Morrison PR, Clerk A, Sugden PH: Phenylephrine promotes phosphorylation of Bad in cardiac myocytes through the extracellular signal-regulated kinases 1/2 and protein kinase A. J Mol Cell Cardiol 2002, 34:749–763
33. Matsui T, Rosenzweig A: Convergent signal transduction pathways controlling cardiomyocyte survival and function: the role of PI 3-kinase and Akt. J Mol Cell Cardiol 2005, 38:63–71
34. Arsic N, Zacchigna S, Zentilin L, Ramirez-Correa G, Pattarini L, Salvi A, Sinagra G, Giacca M: Vascular endothelial growth factor stimulates skeletal muscle regeneration in vivo. Mol Ther 2004, 10:844–854
35. Yano T, Miura T, Whittaker P, Miki T, Sakamoto J, Nakamura Y, Ichikawa Y, Ikeda Y, Kobayashi H, Ohori K, Shimamoto K: Macrophage colony-stimulating factor treatment after myocardial infarction attenuates left ventricular dysfunction by accelerating infarct repair. J Am Coll Cardiol 2006, 47:626–634
36. Rutanen J, Rissanen TT, Markkanen JE, Gruchala M, Silvennoinen P, Kivela A, Hedman A, Hedman M, Heikura T, Orden MR, Stacker SA, Achen MG, Hartikainen J, Yla-Herttuala S: Adenoviral catheter-mediated intramyocardial gene transfer using the mature form of vascular endothelial growth factor-D induces transmural angiogenesis in porcine heart. Circulation 2004, 109:1029–1035
37. Azuma J, Taniyama Y, Takeya Y, Iekushi K, Aoki M, Dosaka N, Matsumoto K, Nakamura T, Ogihara T, Morishita R: Angiogenic and antifibrotic actions of hepatocyte growth factor improve cardiac dysfunction in porcine ischemic cardiomyopathy. Gene Ther 2006, 13:1206–1213
38. Bhatt NY, Kelley TW, Khramtsov VV, Wang Y, Lam GK, Clanton TL, Marsh CB: Macrophage-colony-stimulating factor-induced activation of extracellular-regulated kinase involves phosphatidylinositol 3-kinase and reactive oxygen species in human monocytes. J Immunol 2002, 169:6427–6434
39. Gobert Gosse S, Bourgin C, Liu WQ, Garbay C, Mouchiroud G: M-CSF stimulated differentiation requires persistent MEK activity and MAPK phosphorylation independent of Grb2-Sos association and phosphatidylinositol 3-kinase activity. Cell Signal 2005, 17:1352–1362
40. Lipovetsky G, Fenoglio JJ, Gieger M, Srinivasan MR, Dobelle WH: Coronary artery anatomy of the goat. Artif Organs 1983, 7:238–245

Proceedings of the 29th Annual International
Conference of the IEEE EMBS
Cité Internationale, Lyon, France
August 23-26, 2007.

Quantitative Evaluation for Anastomotic Technique of Coronary Artery Bypass Grafting by using In-vitro Mock Circulatory System

Young Kwang Park, Yutaka Mita, Eriko Oki, Naohiko Kanemitsu, Yasuyuki Shiraishi, Yousuke Ishii, Takashi Azuma, Masami Ochi, and Mitsuo Umezu, *Member, IEEE*

Abstract—**This study focuses on the development of self-training system for surgical operation and quantitative evaluation of the surgical skills. Our group has developed a self-training system for anastomotic technique in Coronary Artery Bypass Grafting (CABG) to contribute the education of cardiovascular surgery without a risk to patients. The self-training system consists of following portions, 1) "YOUCAN", coronary and graft vascular silicone model, 2) "BEAT", a device, simulating stabilized myocardial surface, and 3) Quantitative evaluation system based on *in vitro* mock circulatory system. The coronary and graft model has been anastomosed by expert and trainee cardiac surgeon. The anastomosed model was mounted onto test section of the *in vitro* mock circulatory system then identical waveforms of coronary artery was applied into the inlet of an anastomosis. The energy loss was quantified as a pressure difference between proximal and distal ends of anastomosis. The energy loss was obtained as 67.3±1.75mJ (trainee) and 41.3±3.08mJ (registered surgeon). It was founded that average energy loss by expert surgeon was lower by 38.6% than that by trainee surgeon. The major difference among the models of expert and trainee was the Effective Orifice Area (EOA) of the anastomosis. Through the experiment, EOA was confirmed by image analysis as 2.73 mm^2 for an expert against 0.534 mm^2 for a trainee. In conclusion, it was suggested that the anastomotic skill among expert and trainee surgeons could be hydrodynamically differentiated by using *in vitro* mock circulatory system.**

I. Introduction

ACCORDING to a statistical survey, there are 2,937 registered cardiac surgeons in Japan, whereas number of CABG cases was 20,095 in 2002 in Japan [1]. In other word, only 7 cases per one cardiac surgeon were performed in a year. The above data shows that situation is difficult to train trainee surgeons through the only clinical experience in operating theater. Training surgeons in a routine surgical operation is becoming difficult especially in a field of cardiovascular surgery from the view point of risks of medical safety for patients. To overcome the situation, alternative training program has been started in Japan. Fig.1 shows recently started surgical training program named WETLAB. Defrosted porcine hearts are installed into a simple cavity model. Registered surgeons closely teach surgical techniques to trainee surgeons. The advantages of the WETLAB are 1) understanding anatomy, 2) a real tactile feeling, and 3) no risk to patient. This training program is founded as effective and continually organized by major medical device companies under an indication of the academic society. Fig.2 shows the concept of staged surgical training system, which our group proposes. The DRYLAB stage has been set to complement the WETLAB stage. Artificial patient models and simulators are used instead of animal organs in the DRYLAB. The major difference of the both stages is that the DRYLAB provides self-training against the WETLAB provides group training. In fact, the WETLAB is effective training method, because the evaluation has been immediately done by supervisors. However, it is difficult to organize, daily. On the other hand,

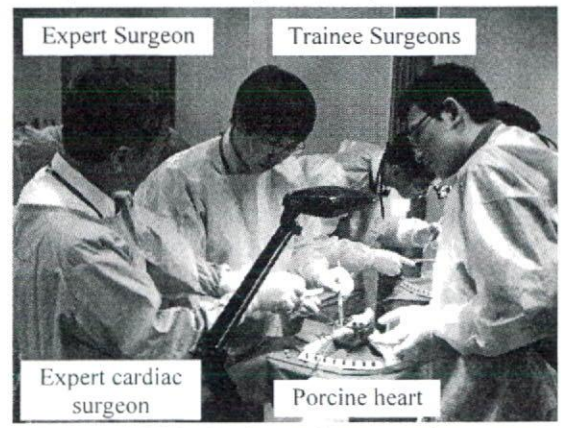

Fig.1. WETLAB in ordinary seminar room: Supervisor gives technical advice to trainee surgeons.

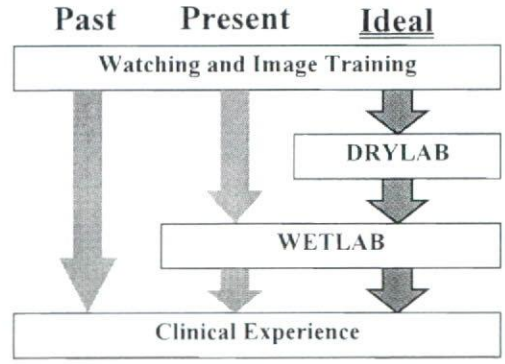

Fig.2. The concept of staged surgical training system.

This work was partly supported by "the robotic medical technology cluster in Gifu prefecture", Knowledge Cluster Initiative, Ministry of Education, Culture, Sports, Science and Technology, Japan, and also partly supported by the 21st Century Center of Excellence (COE) Program "The innovative research on symbiosis technologies for human and robots in the elderly dominated society", Waseda University, Tokyo, Japan.

Y. Park is affiliated with Major in Integrative Bioscience and Biomedical Engineering, Graduate School of Waseda University, 58-322, 3-4-1 Ohkubo, Shinjuku-ku, Tokyo, Japan
(corresponding author to provide phone +81-3-5286-3256, fax +81-3-3200-2516, e-mail youngpark@moegi.waseda.jp).

1-4244-0788-5/07/$20.00 ©2007 IEEE

the DRYLAB is adequate method for daily repetitive training of basic surgical skills. However, an alternative is needed for self-training in the DRYLAB stage instead of the supervisors.

II. Objective

The purpose of this study is a development of the self-training system for surgical technique. The first stage of the study, our group develops the self-training system for anastomotic technique of CABG, which is used in the DRYLAB then differentiates surgical skills of expert and trainee surgeon by using newly developed evaluation system.

III. Development

The self-training system consists of following portions, 1) "YOUCAN", coronary and graft vascular silicone model, 2) "BEAT", a device, simulating stabilized myocardial surface, and 3) Quantitative evaluation system based on *in vitro* mock circulatory system.

A. Coronary artery and graft model "YOUCAN"

These models provide repetitive anastomotic training under static condition as shown in fig.3. An anastomosis between Left Anterior Descending coronary artery (LAD) as recipient and Left Internal Thoracic Artery (LITA) as graft has been simulated by these models, because it is the most common combination for CABG. Inner diameter of the model is 2.0mm and the models are made of silicone rubber (KE1603 A/B, Shin-Etsu chemical co. ltd). Elasticity of the models was controlled to satisfy the surgeons' tactile feeling reasonably, by the ratio of compounded silicone oil [2]. Tethering, a self-expandable function of incised part was reproduced by remaining stress in myocardial model. Therefore surgeon could handle a surgical needle and strings as if under the clinical condition.

B. Off-Pump CAB training device "BEAT"

Fig.4 shows Off-Pump CAB training device named BEAT. Off-Pump CAB is CABG under on-beating condition avoiding the invasiveness derived from extracorporeal circulation. The BEAT adds pulsatile up-and-down uniaxial motion of stabilized myocardial surface onto the coronary model [3]. Biometal, shaped memory alloy developed by TOKI Corp, has been employed as the actuator because of the compactness and controllability. The heart rate and amplitude were adjustable between 50~100 bpm (0.83~1.67 Hz) and 0~3mm as a trainee surgeon desired by the controller. Various coronary arterial positions, including LMT, LAD, RCA, and Cx, could be set by the attitude adjuster, which is flexible ball joint. The surgical field was simulated by cavity unit. By the development of above portions, our group could provide a DRYLAB environment to train the anastomotic technique under the fixed condition.

C. in vitro Coronary Circulatory System

Fig.5 shows the evaluation system for anastomosed model based on in vitro Coronary Circulatory System (CCS). CCS had been originally developed by Kawai et. al. in 2004[4]. It is composed of the systemic circulatory system and the CCS.

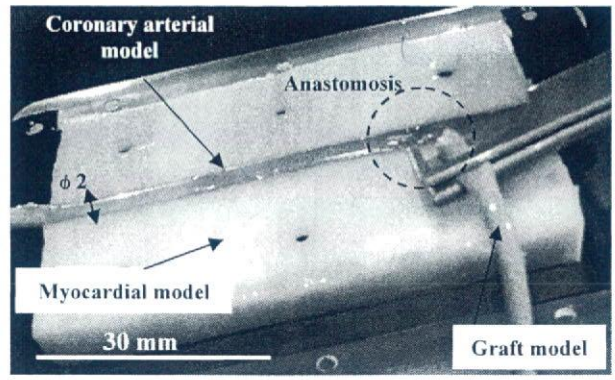

Fig.3. Coronary arterial model" YOUCAN" and graft model of silicone rubber, which elasticity had been

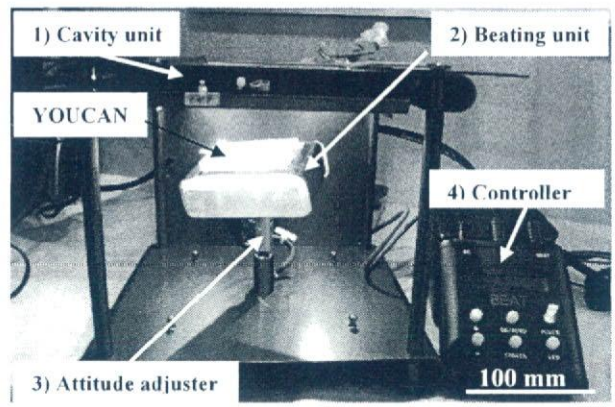

Fig.4. Off-Pump CAB training device "BEAT"

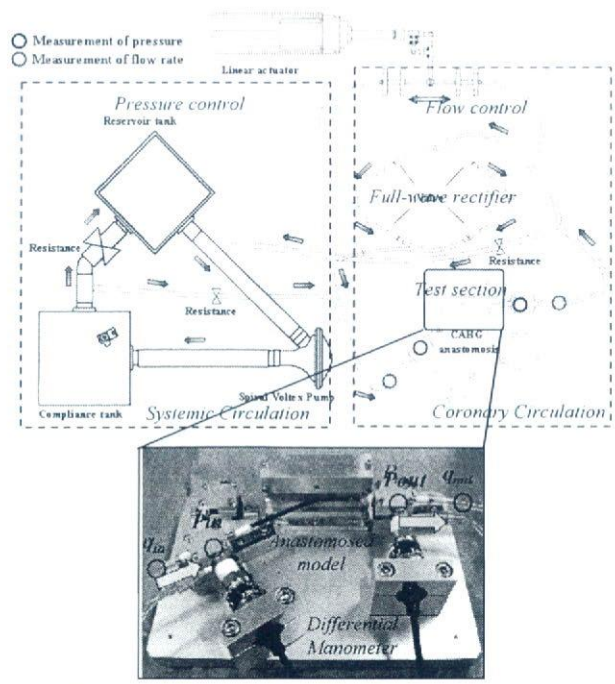

Fig.5. *in vitro* Coronary Circulatory System for hydrodynamic evaluation of the anastomosed model

The CCS, driven by linear actuator composed of stepping motor, has been designed to reproduce natural coronary hemodynamics. Pressure and flow rate were measured at the inlet and outlet of the test section. Differential manometer (AP-12S, KEYENCE) was installed to measure pressure loss of vicinity of the anastomosis.

IV. Evaluation

Our group has conducted the experiment to clarify the difference among expert and trainee surgeon's skills by using above newly developed self-training system as shown in Fig.5. A registered cardiac surgeon was selected as the expert surgeon. And a cardiac surgeon, who has never been an operator in clinical has been selected as the trainee surgeon. The both expert and trainee surgeon anastomosed the coronary artery and graft model, which was set onto the BEAT under non beating condition. The anastomosed model s were set onto the test section of the CCS. Identical waveforms in coronary artery were applied into the inlet of the anastomosis under the following conditions, 120/80mmHg of pressure (normotension), 53ml/min of mean flow rate. Pressure and flow rate were measured at proximal and distal ends of the anastomosis. Then energy loss was calculated by equation (1), using the following parameters: pressure gradient ΔP and flow rate Q_m

$$E_{loss} = \oint (\Delta P \cdot Q_{in}) dt \qquad (1)$$

V. Result and Discussion

Our group considered the experimental results in terms of relevance between morphological and hydrodynamics characteristics of the bypass grafting anastomosis.

A. Morphological characteristics

Fig.6 shows comparative visual inspection of the anastomosis, which has been done by the expert and the trainee surgeon. The both models were anastomosed by continuous suture using PROLENE 7-0 (Ethicon Inc.). In the overhead view of anastomosis, it was observed that intervals of each stitch were regular in expert surgeon's anastomosis. Moreover, a length of each stitch was nearly equal and its direction was almost normal to the suture line. In contrast, the orientation of each stitch was irregular in the trainee's anastomosis. The irregular stitch was caused to configuration of the collapsed orifice area, which is pointed with dotted line in Fig.6. In the frontal view of the anastomosis, expert model has an outline of the graft model, which straightly and smoothly connected to the coronary artery. On the other hand, an outline of the graft model in trainee model was formed as downhill in part. It was observed that a cross-stitch was on the suture line in collapsed orifice area in trainee's anastomosis. The cross-stitch may cause to stenotic pattern of an inner lumen. In order to investigate a shape of inner lumen, wax injection molding has done as shown in Fig.7. Then, Effective Orifice Area (EOA) has been quantified by image analysis on cross-sectional surface of the anastomosis. As the result, which was shown in TABLE I, an EOA of the trainee model has been calculated as 19.4% of the expert model. The effect of this difference of EOA to hydrodynamics in the anastomosis has been considered in next section.

B. Hydrodynamic effect to an anastomosis

Fig.8 shows natural waveforms of pressure and flow rate in a coronary artery. It was confirmed that the typical double-peaked waveforms of flow rate and single-peaked waveforms in coronary artery were reproduced by CCS as shown in Fig.9. Pressure loss could be found from the difference between waveforms of inlet and outlet pressure in the both expert and trainee models. Then, energy loss was calculated as 41.30 ± 3.08mJ for the expert and 67.28 ± 1.75mJ for the trainee surgeon as shown in Fig.10. The energy loss of the expert surgeon was 38.6% less than the trainee surgeon. If we discuss the anastomotic models as bended tubular shaped elastic model, a drastic change of the EOA may be cause of a significant pressure gradient on tubular axis between inlet and outlet of the tube. It was inferred that this pressure gradient affects to separate the local flow of near vascular wall. Thus, it was thought as that energy loss of the trainee model was higher than the expert model.

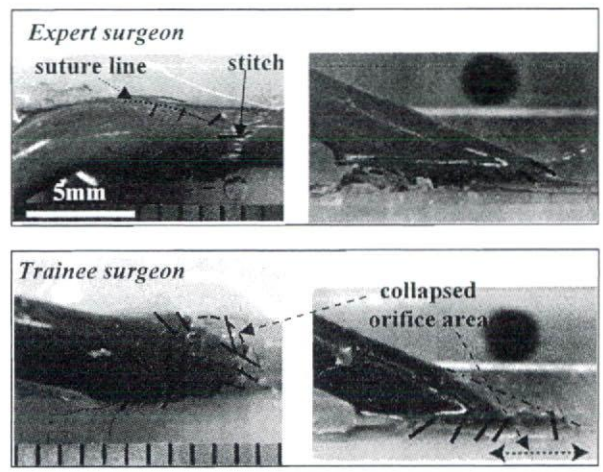

Fig.6. Appearance of anastomosed model of the expert and the trainee.

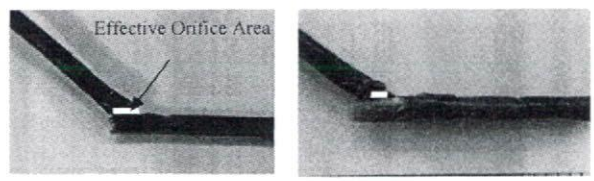

(a) Expert model (b) Trainee model

Fig.7. Inner geometry of anastomosed model, fabricated by wax injection molding.

TABLE I
Effective Orifice Area of Expert and Trainee Model

Class	EOA (mm^2)
Expert surgeon	2.73
Trainee surgeon	0.53

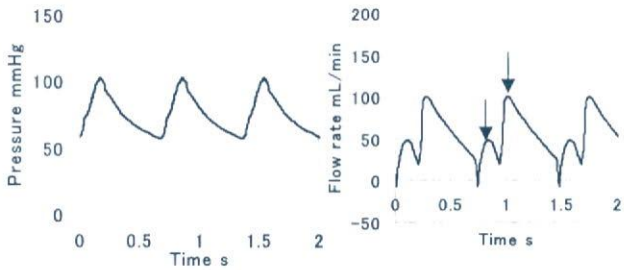

Fig.8. Natural waveforms of pressure and flow rate in a coronary artery (hypotension)

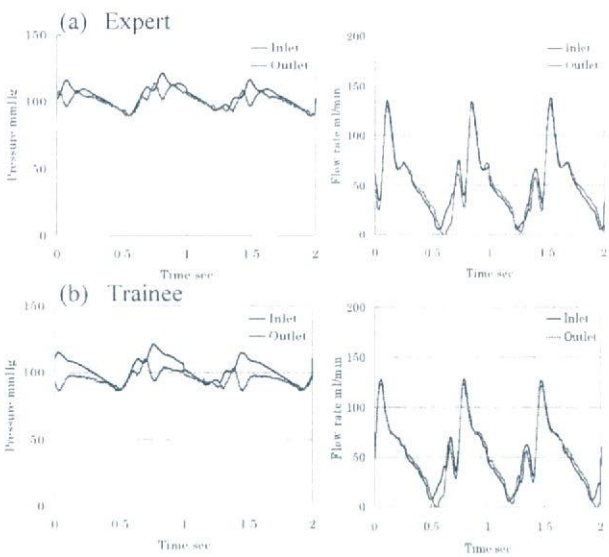

Fig.9. Waveforms of pressure and flow rate at the inlet and outlet of the anastomosed model

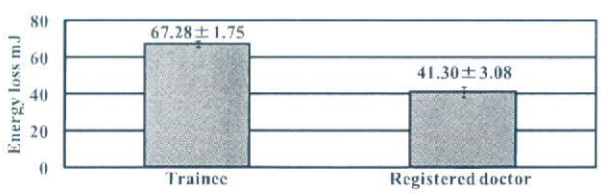

Fig.10. Energy loss for the trainee and the expert (registered) surgeon's anastomosis.

This experimental result implies that the technique of controlling EOA is relevant to improve the hydrodynamic characteristics of the anastomosis. The further study is required to clarify the characteristics of these local flows by using flow visualization technology such as Particle Image Velocimetry.

VI. Conclusion

In this study, a self-training system for the anastomotic technique in CABG has been developed. The selected expert and trainee surgeon's anastomotic skill has been differentiated by using the coronary circulatory system. Throughout the visual inspection, it was observed that the orientation of the trainee surgeon's each stitch was irregular, comparing to expert surgeon. This has caused to narrow EOA, and then the higher energy loss has been induced in the trainee anastomosis. In conclusion, it has been suggested that an expert and a trainee surgeon's anastomosis could be differentiated by using *in vitro* mock circulatory system. We will continue studying to reveal an essence of expert surgeons' skills by following approaches. The one is statistic analysis of the anastomotic technique to find typical pattern among expert and trainee surgeons. The other is considering the relation between configuration of the EOA in an anastomosis and the hydrodynamic characteristics by analyzing local flow. It is expected that these study will contribute to the establishment of an evaluative criteria for human surgeons and robot surgeons in the future.

Acknowledgment

This work was partly supported by "the robotic medical technology cluster in Gifu prefecture", Knowledge Cluster Initiative, Ministry of Education, Culture, Sports, Science and Technology, Japan, and also partly supported by the 21st Century Center of Excellence (COE) Program "The innovative research on symbiosis technologies for human and robots in the elderly dominated society", Waseda University, Tokyo, Japan.

References

[1] the Ministry of Health, labour and welfare, "statistical survey on medical doctors",2002

[2] Y. Park, K. Nishikawa, Y. Mita, E. Oki, M. Uematsu, Y. Shiraishi, H. Takemura, H. Yaku, K. Kawazoe, A. Takanishi and M. Umezu, "Development of "Patient Robot": Surgical Training Machine for Off-Pump Coronary Artery Bypass Grafting", the 12th of International Confference on Biomedical Engineering 2005, Dec, 2005

[3] Uematsu M., Shiraishi Y., Park Y., Umezu M. et al. (2005): 'An approach to analyse the stress distribution on the cardiac surface using optical measurement', *Japan Soc. ME & BE*, **43**, pp. 45

[4] M. Umezu, J. Kawai, J. Suehiro, M. Arita, Y. Shiraishi, K. Iwasaki, T. Tanaka, T. Akutsu, H. Niinami, "Biomedical engineering analysis on the effectiveness of cardiovascular surgery anastomosis methods for coronary artery bypass grafting", 7th Polish – Japanese seminar on new technologies for future artificial organs, Sep, 2004, pp 80-86

J Artif Organs (2007) 10:223–227
DOI 10.1007/s10047-007-0395-y

ORIGINAL ARTICLE

Hongjian Liu, PhD · Yun Luo, PhD · Masaru Higa, PhD
Xiumin Zhang, PhD · Yoshifumi Saijo, MD, PhD
Yasuyuki Shiraishi, PhD · Kazumitsu Sekine, PhD
Tomoyuki Yambe, MD, PhD

Biochemical evaluation of an artificial anal sphincter made from shape memory alloys

Abstract Severe anal incontinence is a socially incapacitating disorder and a major unresolved clinical problem that has a considerable negative impact on quality of life. In this study, we developed a new artificial anal sphincter using shape memory alloys (SMAs) in order to improve the quality of life of such patients and evaluated the influence of this sphincter on blood serum chemistry in animal experiments. The artificial anal sphincter was driven by two Ti-Ni SMA actuators sandwiching the intestine and was implanted in three female goats. Blood was collected from the jugular vein on days 1 and 4; at weeks 1 and 2; and at months 1, 2, and 3, postoperatively. Biochemical parameters including total protein, albumin, total bilirubin, aspartate aminotransferase, blood urea nitrogen, creatinine, and C-reactive protein were examined. The time courses of total bilirubin and aspartate amino transferase of the three goats were within the baseline levels after 1 week of implantation and remained normal, demonstrating no liver function complications. The blood urea nitrogen and creatinine levels remained within the normal range, indicating no renal function complications. The total protein and albumin fluctuated within the normal range throughout the duration of this study. In these goats, it was also found that the level of C-reactive protein did not increase and that there was no stricture of the intestine where the artificial sphincter was attached. Our findings indicate that the artificial sphincter SMA demonstrated no adverse influence on blood serum chemistry and exhibited an effective system performance.

Key words Shape memory alloys · Artificial anal sphincter · Biochemical evaluations · Implantation · Goat

Introduction

Severe anal incontinence (incontinence for gas, feces, or both) is a socially incapacitating disorder and a major unresolved clinical problem that has a considerable negative impact on quality of life. This condition is caused by colostomy or ileostomy, neuromuscular disorders, congenital anorectal malformation, and obstetric injury.[1] As a treatment for such patients, an artificial anal sphincter (AMS800, American Medical Systems, Minneapolis, MN, USA) was developed and has been implanted in animal models and patients. However, it has been indicated that the artificial sphincter may not withstand prolonged use because of mechanical failure and structures using a liquid drive mechanism.[1,2]

Nickel–titanium (Ni-Ti) shape memory alloys (SMAs) have many unique mechanical and material characteristics combined with good biocompatibility. SMAs are attracting considerable attention as core materials in medical applications because of their high ratio of recovery force to weight and large recoverable strains. SMAs are durable and can endure up to 50000 cycles of heating and cooling.[3,4] We have previously reported the development of artificial anal sphincters using SMAs for treating patients with neuromuscular disorders, severe congenital anomalies, or colostomy.[3,5] The artificial anal sphincter has only one deformable part and therefore has a simple structure with good durability and is expected to reduce the possibility of mechanical failure. In this study, we evaluated the influence of the artificial anal sphincter on blood serum chemistry in animal experiments.

Received: March 6, 2007 / Accepted: July 31, 2007

H. Liu (✉) · Y. Saijo · Y. Shiraishi · K. Sekine · T. Yambe
Department of Medical Engineering and Cardiology, Institute of Development, Aging and Cancer, Tohoku University, 4-1 Seiryo-machi, Aoba-ku, Sendai 980-8575, Japan
Tel. +81-22-717-8517; Fax +81-22-717-8518
e-mail: hongjianliu63@yahoo.co.jp

Y. Luo · M. Higa
Biomedical Engineering Research Organization, Tohoku University, Sendai, Japan

X. Zhang
Department of Medicine and Science in Sports and Exercise, Tohoku University Graduate School of Medicine, Sendai, Japan

Materials and methods

Animals

Three female goats weighing 50–60 kg were used. The animal experiments were performed after approval by the Research Animal Resource Committee of the Institute of Experimental Animals, Tohoku University School of Medicine, Japan.

Artificial anal sphincter device

The artificial sphincter (AS) is driven by two Ti-Ni SMA actuators sandwiching the intestine. The composition of SMA used in this study was Ti51at%Ni on an atomic basis. The actuator consists of two SMA plates ($70 \times 18.5 \times 0.7$ mm) jointed by hinges at their ends and foil type heaters attached on the SMA plates. Silicone pillows were placed on the surfaces of the SMA plates to prevent pressure concentration on the intestines, which may cause ischemia. The bilateral ends of two SMA plates of circumferential shape were fixed with latches, and the alimentary tract was placed between the two SMA actuators.

To control the opening and closing of the anal canal, two meander winding 0.2-mm wires were attached on the surface of each SMA plate as heaters. On heating, the reverse R-phase transformation occurred in the SMA plates, accompanied by shape changes from a flat shape to an arc shape. The shape change resulted in a lumen between the two SMA plates, which allowed bowel movement to take place.

The power to heat the SMA plates can be provided percutaneously by a DC/AC external power supply. A transcutaneous energy transmission system (TETS) was used to supply power to the AS. This system consisted of two coils, one outside the body (primary coil) and the other inside the body (secondary coil). A temperature-responsive reed switch (TRS, TDK, TR-55B50, Tokyo, Japan) was used to prevent overheating of the AS. When an electric current of 4 A at 4 V was supplied, the temperature of the SMA plates immediately started to rise, and the two plates bent to form an almond shape at a temperature of 55°C with a maximal gap of 33 mm between the plates. When the electric current was removed, the SMA plates recovered their initial shapes on natural cooling, resulting in closure of the intestines once again (Fig. 1).

Implantation of the artificial anal sphincter

The animals were placed on a surgical table in the lateral position under general anesthesia and were prepped and draped in sterile fashion. Anesthesia applied by halothane inhalation via a respirator was maintained throughout the procedure.

The creation of end-colostomy on the abdomen through the oblique muscles and the implantation of the artificial SMA anal sphincter were performed. The artificial anal sphincter and overheating protector were implanted between the peritoneum and abdominal wall. The colostomy was reached via an extraperitoneal approach and a space around it was created. The artificial anal sphincter was attached to the intestine with latches. The secondary coil

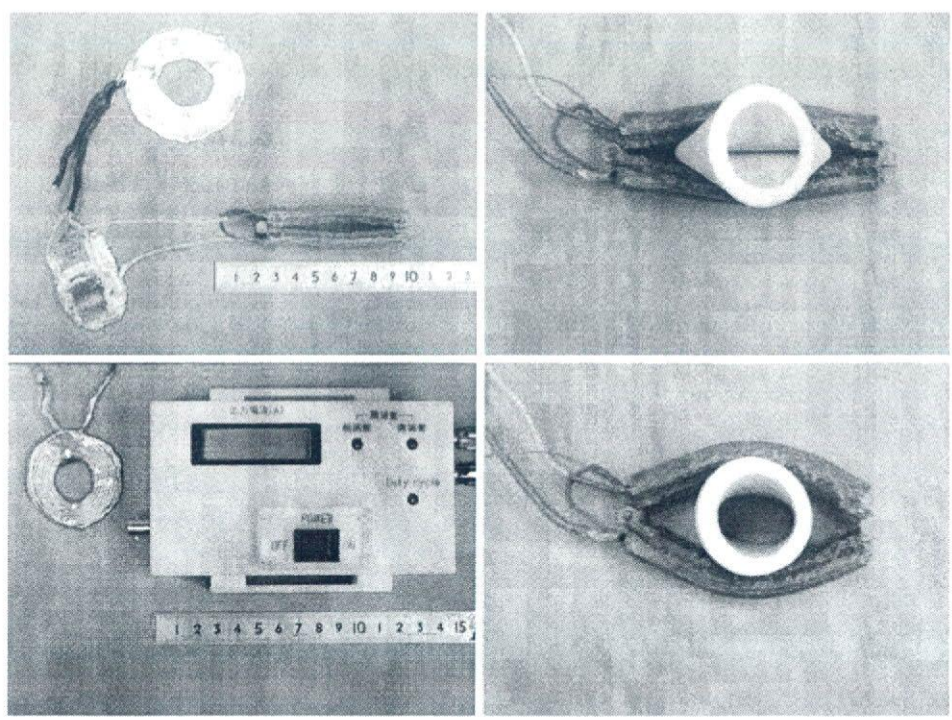

Fig. 1. Implantable components and transcutaneous energy transmission system of a shape memory alloy (SMA) artificial sphincter (AS). *Top left*, implanted components; *bottom left*, extracorporeal components; *top right*, closed state; *bottom right*, open state

was placed in the subcutaneous space near the colostomy, and the primary coil was attached to the skin, aligned with the secondary coil (Fig. 2). The lines to supply electric current to the device were led outside through a subcutaneous tunnel. An antibiotic was administrated intravenously for 3 days after surgery, and feeding was started on the day after the surgery. The bowels of the goats were moved 10 times a day by supplying electricity to the primary coil for 10 min.

Test of biocompatibility

Blood was collected from the jugular vein on days 1 and 4; at weeks 1 and 2; and at months 1, 2, and 3, postoperatively. The blood was centrifuged at 3000 rpm for 10 min to obtain the blood components from the supernatant for hematological examinations. Biochemical parameters including total protein, albumin, total bilirubin, aspartate aminotransferase (AST), blood urea nitrogen, creatinine, and C-reactive protein (CRP) were examined. The animals were killed 3 months after surgery under anesthesia, and tissue samples were collected from the intestine, liver, and kidneys and were preserved in 10% formalin.

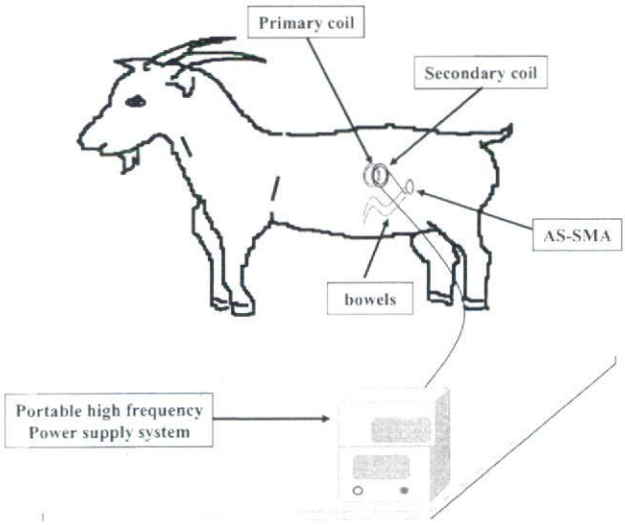

Fig. 2. Chronic animal experiment of a goat implanted with the AS-SMA

Results

In this study, the duration of the three long-term implants of the artificial anal sphincter (i.e., more than 1 week) ranged from 30 to 90 days. The data at 3 months from two of the goats could be recorded; however, the third goat was eliminated from the trial one month after the procedure due to failure of the electrodes.

The device was operated 300 times in 1 month; bowel movements were observed and the stools appeared the same as those seen before implantation. The stoma was always continent in the resting position of the AS, and the goats had a good appetite with no abdominal distension. Macroscopically, the stoma had a ruddy complexion and exhibited elasticity; there was no stricture of the intestine where the AS was attached.

Throughout the study period, the major biochemistry parameters were almost always within the normal ranges. The time courses of total bilirubin and AST of the three goats were within the baseline levels after 1 week of implantation and remained normal, indicating that there were no liver function complications (Fig. 3). The blood urea nitrogen and creatinine levels of the three goats remained within the normal range, demonstrating no renal function complications (Fig. 4). The total protein and albumin levels fluctuated within the normal ranges throughout the study period (Fig. 5), and in these goats, we also found that the level of CRP had not increased during the study.

The developed SMA artificial sphincter (AS-SMA) was implanted in animal models for chronic experiments of up to 3 months duration and exhibited good performance in maintaining fecal continence.

Discussion

The normal biochemistry results observed throughout this study bodes well for the future clinical use of the AS-SMA. Different hematological parameters were evaluated for in vivo assessment of biochemistry. The effects of the AS-SMA on renal and liver functions were evaluated by changes in total creatinine, blood urea nitrogen, bilirubin, and AST. In one goat, abnormal AST and bilirubin levels were evident on postoperative day 4, but these had returned to the normal range by postoperative day 7. The use of halothane anes-

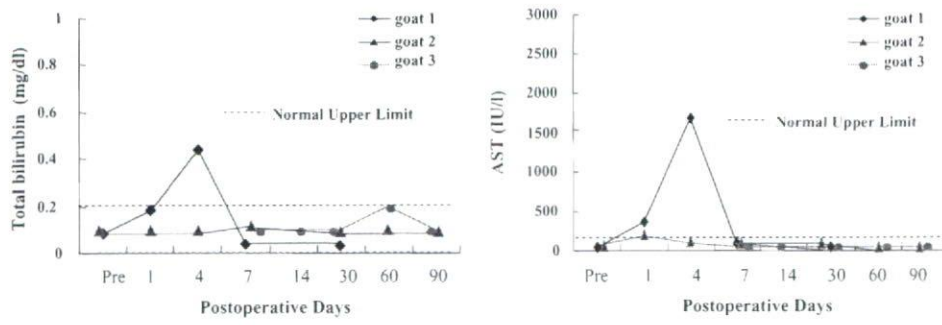

Fig. 3. Total bilirubin and aspartate aminotransferase (*AST*) levels as markers of liver function

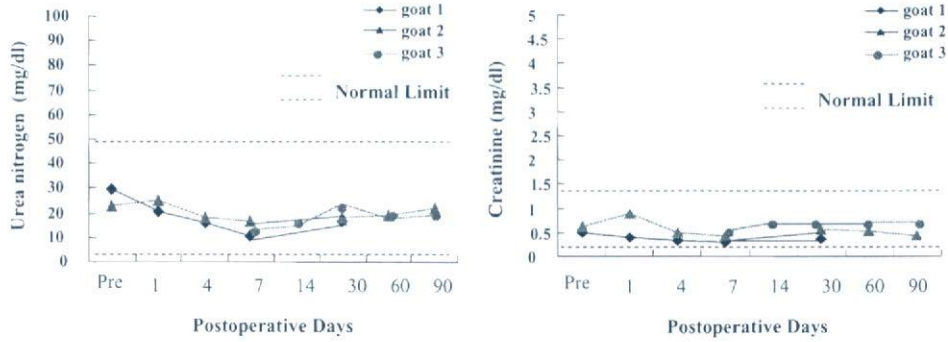

Fig. 4. Urea nitrogen and creatinine levels as markers of renal function

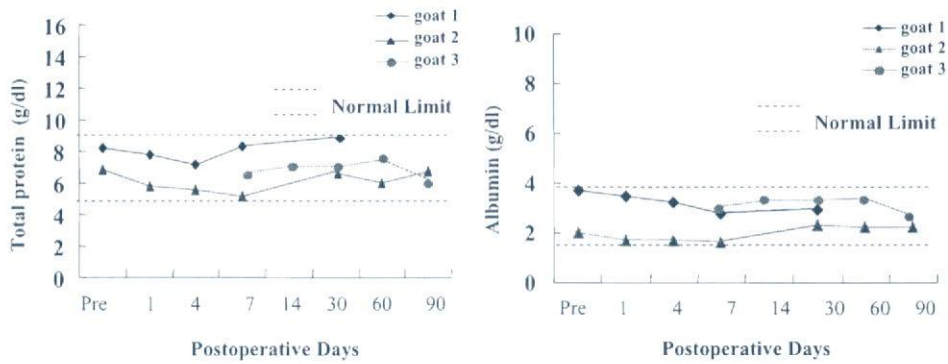

Fig. 5. Total protein and albumin levels as markers of nourishment state

thesia can induce an elevation of serum activities of liver enzymes, often around 2 to 7 days after anesthesia, and the leakage of enzyme into the serum may have come from muscle damage at the time of surgery.

Chronic in vivo studies of the AS-SMA in three goats demonstrated little influence on blood serum chemistry and showed the reliability and effective performance of the system. There were no incidences of bleeding, systemic organ dysfunction, or mechanical failure in any of the goats. Of the three long-term implanted goats, one goat was terminated after 30 days because of electrode-related issues, and two goats were terminated after 90 days. The failure of the electrodes was consistent with moisture permeation; device-related difficulties were limited to just two cable-related issues.[6–12]

Use of this AS-SMA will minimize the surgical invasiveness and compression of the surrounding tissues such as the skin and gastrointestinal system, resulting in a rapid recovery from the surgery and reduced risks of pocket bleeding, wound infection, and malnutrition. Ni-Ti alloys have been reported to exhibit good biocompatibility due to their high corrosion resistance and Ni-Ti alloys have gained popularity in the biomedical field because of their appealing mechanical properties.[11,13–15] The SMA was covered with a silicone pillow and exhibited conformity with the living body in the contact point with the anal canal. The soft silicone pillow covering material reduces the pressure concentration on the contacting area of the intestines and allows good circulation.

In this study, the small loss of power by the TETS resulted in sufficient capability for energy transmission. During the experiment, the AS opened each time energy was transmitted; however, if the efficiency were improved, less AC power would be required. The AS was kept open for 10 min, although the surface temperature was lower than 43°C because the allowable body temperature was around 42°C. The overheating protector was able to prevent burns around the AS and extended the duration of AS opening.[1,4,5]

The AS was opened for a long enough period (10 min) to allow controlled fecal continence. Fecal movements were regularly observed when the artificial anal sphincter was activated, and the evacuated feces were confirmed as being normal.

These biochemistry studies support the concept and design of this implantable artificial anal sphincter. In conclusion, this artificial anal sphincter demonstrated no adverse influence on blood serum chemistry and exhibited an effective system performance.

Acknowledgments This research was supported by the Industrial Technology Research Grant Program in 2000 (00A45027) from the New Energy and Industrial Technology Development Organization (NEDO) of Japan.

References

1. Nishi K, Kamiyama T, Wada M, Amae S, Ishii T, Takagi T, Luo Y, Okuyama T, Yambe T, Hayashi Y, Ohi R. Development of an implantable artificial anal sphincter using a shape memory alloy. J Pediatr Surg 2004;39:69–72
2. Hajivassiliou CA, Carter KB, Finlay IG. Biomechanical evaluation of an artificial anal sphincter prosthesis. J Med Eng Technol 1997;21:89–95

3. Amae S, Wada M, Luo Y, Nakamura H, Yoshida S, Kamiyama T, Yambe T, Takagi T, Nitta S, Ohi R. Development of an implantable artificial anal sphincter by the use of a shape memory alloy. ASAIO J 2001;47:346–350
4. Luo Y, Higa M, Amae S, Takagi T, Yambe T, Okuyama T, Tanaka H, Kakubari Y, Matsuki H. Preclinical development of SMA artificial anal sphincters. Minim Invasive Ther Allied Technol 2006; 15:241–245
5. Luo Y, Takagi T, Okuyama T, Amae S, Wada M, Nishi K, Kamiyama T, Yambe T, Matsuki H. Functional evaluation of an artificial anal sphincter using shape memory alloys. ASAIO J 2004;50: 338–343
6. Jain A, Mohanka R, Orloff M, Abt P, Kashyap R, Cullen J, Lansing K, Bozorgzadeh A. University of Wisconsin versus histidine-tryptophan-ketoglutarate for tissue preservation in live-donor liver transplantation. Exp Clin Transplant 2006;4:451–457
7. Mussivand T, Harasaki H, Litwak K, Slaughter MS, Gray LA Jr, Dowling TR, Mueller R, Masters RG, Hendry PJ, Beck-Da-silva L, Davies R, Haddad H, Mesana TG, Keon WJ. In vivo evaluation of the biocompatibility of the totally implantable ventricular assist device (HeartSaver VAD). ASAIO J 2003;49:459–462
8. Ortiz H, Armendariz P, DeMiguel M, Ruiz MD, Alos R, Roig JV. Complications and functional outcome following artificial anal sphincter implantation. Br J Surg 2002;89:877–881
9. Petrou SP, Elliott DS. Artificial urethral sphincter for incontinence in adults. Drugs Today (Barc) 2001;37:237–244
10. Schenk S, Weber S, Luangphakdy V, Flick CR, Chen JF, Inoue M, Kopcak MW Jr, Ootaki Y, Doi K, Dessoffy R, Hirschman GB, Vitale NG, Chapman PA Jr, Smith WA, Fukamachi K. In vivo performance and biocompatibility of the MagScrew ventricular assist device. ASAIO J 2003;49:594–598
11. Vaizey CJ, Kamm MA, Gold DM, Bartram CI, Halligan S, Nicholls RJ. Clinical, physiological, and radiological study of a new purpose-designed artificial bowel sphincter. Lancet 1998;352:105–109
12. Yokus B, Cakir DU, Kanay Z, Gulten T, Uysal E. Effects of seasonal and physiological variations on the serum chemistry, vitamins and thyroid hormone concentrations in sheep. J Vet Med A Physiol Pathol Clin Med 2006;53:271–276
13. Es-Souni M, Es-Souni M, Fischer-Brandies H. On the transformation behaviour, mechanical properties and biocompatibility of two NiTi-based shape memory alloys: NiTi42 and NiTi42Cu7. Biomaterials 2001;22:2153–2161
14. Thierry B, Tabrizian M, Trepanier C, Savadogo O, Yahia L. Effect of surface treatment and sterilization processes on the corrosion behavior of NiTi shape memory alloy. J Biomed Mater Res 2000; 51:685–693
15. Wilson SK, Delk JR II. Ectopic placement of AMS 800 urinary control system pressure-regulating balloon. Urology 2005;65: 167–170

Biocybernetics and Biomedical Engineering
2007, Volume 27, Number 1/2, pp. 45–52

Development of Implantable Probe for Observation of Microcirculation

KOU IMACHI[1,*], SHUICHI MOCHIZUKI[3], ATSUSHI BABA[1], TAKASHI ISOYAMA[4], ITSURO SAITO[5], KOKI TAKIURA[6], TSUNEO CHINZEI[5], YASUYUKI SHIRAISHI[2], TOMOYUKI YAMBE[2], YUSUKE ABE[4]

[1] *TUBERO, Tohoku University, Sendai, Japan*
[2] *IDAC, Tohoku University, Sendai, Japan*
[3] *Department of Biomedical Engineering, Osaka Institute of Technology, Japan*
[4] *Department of Biomedical Engineering, Graduate School of Medicine, University of Tokyo, Japan*
[5] *RCAST, University of Tokyo, Japan*
[6] *Faculty of Engineering, Yamagata University, Japan*

It is a long-term controversial point between the circulatory physiologists and the artificial heart researchers whether the pulsatile flow is essential for the living body or not [1]. In particular, since the axial flow pump, a continuous flow pump, that could keep the patients alive for more than a few years was introduced into use in clinical setting in 2001, this problem has been regarded as a very important physiological and pathophysiological issue. The objective of this study was to develop an implantable probe to observe microcirculation in artificial circulation.
The principle of the probe developed in this study is the following: a thin living tissue is put directly on a highly integrated CCD (charge coupled device), and it is illuminated from the backside of the tissue with LED(light emitting diode). The microvascular nets in the tissue will be projected on the CCD surface, like a contact photograph, which produces an image on the TV screen. The problems are how to magnify them to be able to observe the erythrocyte flow, how to control the focus, how to electrically insulate them and how to make them compact.
After several attempts to magnify the image, a micro lens having 2 mm in diameter, 2 mm long and 6 times magnification, was designed and made of acrylic resin. The lens was installed into a CCD camera with 8 mm in diameter and it was 60 mm long. The camera could magnify the image about 650 times on the 14 inches TV screen. A distinct microcirculation image, including the capillary flow, could be observed when the camera was implanted into the connective tissue under the skin of the rabbit. Now the focus control system is being developed with the camera to be implanted in animals on the long-term base.

K e y w o r d s: microcirculation, pulsatility, continuous flow, CCD (charge coupled devise), artificial heart

* Correspondence to: Kou Imachi, TUBERO, Tohoku University, 2-1 Seiryo-machi, Aoba, Sendai, Miyagi, 980-8575 Japan, e-mail: imachi@tubero.tohoku.ac.jp